Rotational Excitation of HC_3N by H_2 and He at low temperatures

Michael Wernli, Laurent Wiesenfeld, Alexandre Faure, Pierre Valiron

Astronomy & Astrophysics manuscript no. HC3N˙revise.hyper24816
November 27, 2006

Rotational Excitation of HC_3N by H_2 and He at low temperatures

M. Wernli, L. Wiesenfeld, A. Faure, and P. Valiron

Laboratoire d'Astrophysique de l'Observatoire de Grenoble, UMR 5571 CNRS/UJF, Université Joseph-Fourier, Boîte postale 53, 38041 Grenoble cedex 09, France

Received November 27, 2006/ Accepted

ABSTRACT

Aims. Rates for rotational excitation of HC_3N by collisions with He atoms and H_2 molecules are computed for kinetic temperatures in the range 5−20 K and 5−100 K, respectively.

Methods. These rates are obtained from extensive quantum and quasi-classical calculations using new accurate potential energy surfaces (PES). The HC_3N – He PES is in excellent agreement with the recent literature. The HC_3N – H_2 angular dependence is approximated using 5 independent H_2 orientations. An accurate angular expansion of both PES suitable for low energy scattering is achieved despite the severe steric hindrance effects by the HC_3N rod.

Results. The rod-like symmetry of the PES strongly favours even ΔJ transfers and efficiently drives large ΔJ transfers. Despite the large dipole moment of HC_3N , rates involving ortho-H_2 are very similar to those involving para-H_2, because of the predominance of the geometry effects. Excepted for the even ΔJ propensity rule, quasi classical calculations are in excellent agreement with close coupling quantum calculations. As a first application, we present a simple steady-state population model that shows population inversions for the lowest HC_3N levels at H_2 densities in the range 10^4−10^6 cm^{-3}.

Conclusions. The HC_3N molecule is large enough to present an original collisional behaviour where steric hindrance effects hide the details of the interaction. This finding, combined with the fair accuracy of quasi classical rate calculations, is promising in view of collisional studies of larger molecules.

Key words. molecular data - molecular processes

1. Introduction

Cyanopolyyne molecules, with general formula $HC_{2n+1}N$, $n \geq 1$, have been detected in a great variety of astronomical environments and belong to the most abundant species in cold and dense interstellar clouds (Bell et al. 1997). One of these, $HC_{11}N$, is currently the largest unambiguously detected interstellar molecule (Bell & Matthews 1985). The simplest one, HC_3N (cyanoacetylene), is the most abundant of the family. In addition to interstellar clouds, HC_3N has been observed in circumstellar envelopes (Pardo et al. 2004), in Saturn satellite Titan (Kunde et al. 1981), in comets (Bockelée-Morvan et al. 2000) and in extragalactic sources (Mauersberger et al. 1990). Furthermore, HC_3N has been detected both in the ground level and in excited vibrational levels, thanks to the presence of low-lying bending modes (e.g. Wyrowski et al. 2003). Owing to a low rotational constant and a large dipole moment, cyanoacetylene lines are thus observable over a wide range of excitation energies and HC_3N is therefore considered as a very good probe of physical conditions in many environments.

Radiative transfer models for the interpretation of observed HC_3N spectra require the knowledge of collisional excitation rates participating to line formation. To the best of our knowledge, the only available collisional rates are those of Green & Chapman (1978) for the rotational excitation of HC_3N by He below 100 K. In cold and dense clouds, however, the most abundant colliding partner is H_2. In such environments, para-H_2 is only populated in the $J = 0$ level and may be treated as a spherical body. Green & Chapman (1978) and Bhattacharyya & Dickinson (1982) postulated that the collisional cross-sections with para-H_2 ($J = 0$) are similar to those with He (assuming thus an identical interaction and insensitivity of the scattering to the reduced mass). As a result, rates for excitation by para-H_2 were estimated by scaling the rates for excitation by He while rates involving ortho-H_2 were not considered.

In the present study, we have computed new rate coefficients for rotational excitation of HC_3N by He, para-H_2 ($J = 0$) and ortho-H_2 ($J = 1$), in the temperature range 5−20 K for He and 5−100 K for H_2. A comparison between the different partners is presented and the collisional selection rules are investigated in detail. The next section describes details of the PES calculations. The cross-section and rate calculations are presented in Section 3. A discussion and a first application of these rates is given in Section 4. Conclusions are drawn in Section 5. The following units are used throughout except otherwise stated: bond lengths and distances in Bohr; angles in degrees; energies in cm^{-1}; and cross-sections in Å^2.

2. Potential energy surfaces

Two accurate interatomic potential energy surfaces (PES) have recently been calculated in our group, for the interaction of HC_3N with He and H_2. Both surfaces involved the same geometrical setup and similar *ab initio* accuracy. An outline of those PES is given below, while a detailed presentation will be published in a forthcoming article.

In the present work, we focus on low-temperature collision rates, well below the threshold for the excitation of the lower bending mode ν_7 at 223 cm^{-1}. The collision partners may thus safely be approximated to be rigid, in order to keep the number of degrees of freedom as small as possible. For small van der Waals complexes, previous studies have suggested (Jeziorska et al. 2000; Jankowski & Szalewicz 2005) that properly averaged molecular geometries provide a better description of experimental data than equilibrium geometries (r_e geometries). For the H_2O – H_2 system, geometries averaged over ground-state vibrational wave-functions (r_0 geometry) were shown to provide an optimal approximation of the effective interaction (Faure et al. 2005a; Wernli 2006).

Accordingly, we used the H_2 bond separation r_{HH} = 1.44876 Bohr obtained by averaging over the ground-state vibrational wave-function, similarly to previous calculations (Hodges et al. 2004; Faure et al. 2005a; Wernli et al. 2006). For HC_3N, as vibrational wave-functions are not readily available from the literature, we resorted to experimental geometries deduced from the rotational spectrum of HC_3N and its isotopologues (Thorwirth et al. 2000; see also Table 5.8 in Gordy & Cook 1984). The resulting bond separations are the following: r_{HC_1} = 1.998385; $r_{C_1C_2}$ = 2.276364; $r_{C_2C_3}$ = 2.606688; r_{C_3N} = 2.189625, and should be close to vibrationally averaged values.

For the HC_3N – He collision, only two coordinates are needed to fully determine the overall geometry. Let $\boldsymbol{R}$ be the vector between the center of mass of HC_3N and He. The two coordinates are the distance $R = |\boldsymbol{R}|$ and the angle θ_1 between the HC_3N rod and the vector $\boldsymbol{R}$. In our conventions, $\theta_1 = 0$ corresponds to an approach towards the H end of the HC_3N rod. For the collision with H_2, two more angles have to be added, θ_2 and ϕ, that respectively orient the H_2 molecule in the rod-$\boldsymbol{R}$ plane and out of the plane. The HC_3N – He PES has thus two degrees of freedom, the HC_3N – H_2 four degrees of freedom.

As we aim to solve close coupling equations for the scattering, we need ultimately to expand the PES function V over a suitable angular expansion for any intermolecular distance R. In the simpler case of the HC_3N – He system, this expansion is in the form:

$$V(R,\theta_1) = \sum_{l_1} v_{l_1}(R)\, P_{l_1}(\cos\theta_1) \quad , \tag{1}$$

where $P_{l_1}(\cos\theta_1)$ is a Legendre polynomial and $v_{l_1}(R)$ are the radial coefficients.

For the HC_3N – H_2 system, the expansion becomes:

$$V(R,\theta_1,\theta_2,\phi) = \sum_{l_1 l_2 l} v_{l_1 l_2 l}(R) s_{l_1 l_2 l}(\theta_1,\theta_2,\phi), \tag{2}$$

where the basis functions $s_{l_1 l_2 l}$ are products of spherical harmonics and are expressed in Eq. (A9) of Green (1975). Two new indices l_2 and l are thus needed, associated respectively with the rotational angular momentum of H_2 and the total orbital angular momentum, see also eq. (A2) and (A5) of Green (1975).

Because the Legendre polynomials form a complete set, such expansions should always be possible. However, Chapman & Green (1977) failed to converge above expansion (1) due to the steric hindrance of He by the impenetrable HC_3N rod, and Green & Chapman (1978) abandoned quantum calculations, resorting to quasi classical trajectories (QCT) studies. Similar difficulties arise for the interaction with H_2. Actually, as can be seen on figure 1 for small R values, the interaction is moderate or possibly weakly attractive for $\theta_1 \sim 90°$ and is extremely repulsive or undefined for $\theta_1 \sim 0, 180°$, leading to singularities in the angular expansion and severe Gibbs oscillations in the numerical fit of the PES over Legendre expansions.

Accordingly, we resorted to a cautious sampling strategy for the PES, building a spline interpolation in a first step, and postponing the troublesome angular Legendre expansion to a second step. All details will be published elsewhere. Let us summarize this first step for He, then for H_2.

For the HC_3N – He PES, we selected an irregular grid in the $\{R,\theta_1\}$ coordinates. The first order derivatives of the angular spline were forced to zero for $\theta_1 = 0, 180°$ in order to comply with the PES symmetries. For each distance, angles were added until a smooth convergence of the angular spline fit was achieved, resulting to typical angular steps between 2 and 15°. Then, distances were added until a smooth bicubic spline fit was obtained, amounting to 38 distances in the range 2.75 – 25 Bohr and a total of 644 geometries. The resulting PES is perfectly suited to run quasi classical trajectories.

We used a similar strategy to describe the interaction with H_2, while minimizing the number of calculations. We selected a few $\{\theta_2,\phi\}$ orientation sets, bearing in mind that the dependence of the final PES with the orientation of H_2 is weak. In terms of spherical harmonics, the PES depends only on $Y_{l_2 m_2}(\theta_2,\phi)$, with $l_2 = 0, 2, 4, \ldots$ and $m_2 = 0, 1, 2, \ldots, |m_2| \leq l_2$. Terms in $Y_{l_2 m_2}$ and $Y_{l_2 -m_2}$ are equal by symmetry. Previous studies (Faure et al. 2005b; Wernli et al. 2006) have shown that terms with $l_2 > 2$ are small, and we consequently truncated the $Y_{l_2 m_2}$ series to $l_2 \leq 2$. Hence, only four basis functions remain for the orientation of H_2 : Y_{00}, Y_{20}, Y_{21} and Y_{22}.

Under this assumption, the whole HC_3N – H_2 surface can be obtained knowing its value for four sets of $\{\theta_2,\phi\}$ angles at each value of R. We selected actually five sets, having thus an over-determined system allowing for the monitoring of the accuracy of the l_2 truncation. Consequently, we determined five independent PES, each being constructed similarly to the HC_3N – He one as a bicubic spline fit over an irregular grid in $\{R,\theta_1\}$ coordinates. The angular mesh is slightly denser than for the HC_3N – He PES for small R distances to account for more severe steric hindrance effects involving H_2 . In total, we computed 3420 $\{R,\theta_1,\theta_2,\phi\}$ geometries. Finally, the HC_3N – H_2 interaction can be readily reconstructed from these five PES by expressing its analytical dependence over $\{\theta_2,\phi\}$ (Wernli 2006).

For each value of the intermolecular geometry $\{R,\theta_1\}$ or $\{R,\theta_1,\theta_2,\phi\}$, the intermolecular potential energy is calculated at

the conventional CCSD(T) level of theory, including the usual counterpoise correction of the Basis Set Superposition Error (Jansen & Ross 1969; Boys & Bernardi 1970). We used augmented correlation-consistent atomic sets of triple zeta quality (Dunning's aug-cc-pVTZ) to describe the HC_3N rod. In order to avoid any possible steric hindrance problems at the basis set level, we did not use bond functions and instead chose larger Dunning's aug-cc-pV5Z and aug-cc-pVQZ basis set to better describe the polarizable (He, H_2) targets, respectively. All calculations employed the direct parallel code DIRCCR12 (Noga et al. 2003-2006).

Comparison of the HC_3N – He PES with existing surfaces (Akin-Ojo et al. 2003; Topic & Wolfgang 2005) showed an excellent agreement. The HC_3N – para-H_2 ($J = 0$) interaction (obtained by averaging the HC_3N – H_2 PES over θ_2 and ϕ) is qualitatively similar to the HC_3N – He PES with a deeper minimum (see values at the end of present Section). As illustrated in Figure 1, these PES are largely dominated by the rod-like shape of HC_3N, implying a prolate ellipsoid symmetry of the equipotentials.

In a second step, let us consider how to circumvent the difficulty of the angular expansion of the above PES, in order to obtain reliable expansions for He and H_2 (eqs 1 and 2).

Using the angular spline representation, we first expressed each PES over a fine θ_1 mesh suitable for a subsequent high l_1 expansion. As expected from the work of Chapman & Green (1977), high l_1 expansions (1) resulted in severe Gibbs oscillations for R in the range 5–7 Bohr, spoiling completely the description of the low energy features of the PES. Then, having in mind low energy scattering applications, we regularized the PES by introducing a scaling function S_f. We replaced $V(R, \theta_1, ...)$ by $S_f(V(R, \theta_1, ...))$, where $S_f(V)$ returns V when V is lower than a prescribed threshold, and then smoothly saturates to a limiting value when V grows up into the repulsive walls. Consequently, the regularized PES retains only the low energy content of the original PES, unmodified up to the range of the threshold energy; it should not be used for higher collisional energies. However, in contrast to the original PES, it can be easily expanded over Legendre functions to an excellent accuracy and is thus suitable for quantum close coupling studies. We selected a threshold value of 300 cm^{-1}, and improved the quality of the expansion by applying a weighted fitting strategy (e.g. Hodges et al. 2004) to focus the fit on the details of the attractive and weakly repulsive regions of the PES. Using $l_1 \leq 35$, both the He and H_2 PES fits were converged to within 1 cm^{-1} for $V \leq 300$ cm^{-1}. These expansions still describe the range $300 < V < 1000$ cm^{-1} to within an accuracy of a few cm^{-1}.

The corresponding absolute minima are the following (in cm^{-1} and Bohr): for HC_3N – He, $V = -40.25$ for $R = 6.32$ and $\theta_1 = 95.2°$; for HC_3N – para-H_2 ($J = 0$), $V = -111.24$ for $R = 6.41$ and $\theta_1 = 94.0°$; and for HC_3N – H_2, $V = -192.49$ for $R = 9.59$, $\theta_1 = 180°$, and $\theta_2 = 0°$.

3. Inelastic cross section and rates

In the following J_1, J_1', denote the initial and final angular momentum of the HC_3N molecule, respectively, and J_2 denote the angular momentum of H_2. We also denote the largest value of J_1, J_1' as J_{1up}.

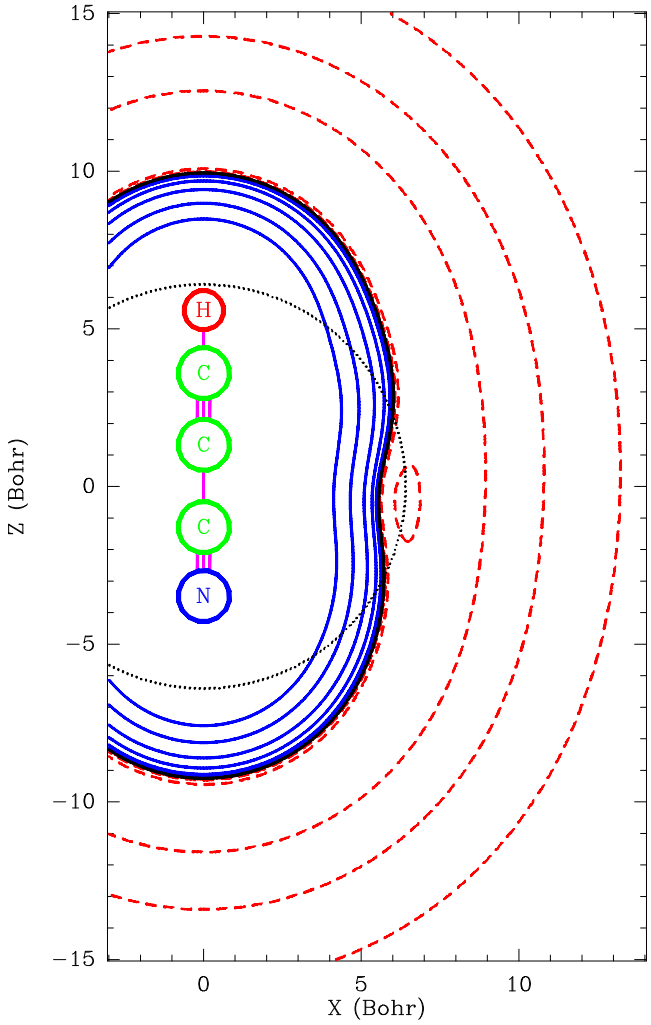

Fig. 1. The HC_3N – para-H_2 PES. The HC_3N molecule is shown at scale. Equipotentials (in cm^{-1}) : in dashed red, -100, -30 -10, -3; in solid black, 0; in blue, 10, 30, 100, 300, 1000, 3000. The dotted circle centered at the HC_3N center of mass with radius $R = 6.41$ Bohr illustrates the angular steric hindrance problem occurring when the collider rotates from the vicinity of the minimum towards the HC_3N rod.

The most reliable approach to compute inelastic cross sections $\sigma_{J_1 J_1'}(E)$ is to perform quantum close coupling calculations. In the case of molecules with a small rotational constant, like HC_3N ($B = 4549.059$ MHz, see e.g. Thorwirth et al. 2000), quantum calculations become soon intractable, because of the large number of open channels involved. While observations at cm-mm wavelengths culminates with $J_{1up} \lesssim 24$ (Audinos et al. 1994), sub-mm observations can probe transition as high as $J_{1up} = 40$, at a frequency of 363.785 GHz and a rotational energy of 202.08 cm^{-1} (Pardo et al. 2004; Kuan et al. 2004; Caux 2006). It is thus necessary to compute rates with transitions up to $J_1 = 50$ ($E = 386.8$ cm^{-1}), in order to properly converge radiative transfer models. Also, we aim at computing rates up to a temperature of 100 K for H_2. We resorted to two methods in order to perform this task. For $J_{1up} \leq 15$, we per-

Table 1. Details of the quantum MOLSCAT cross section calculation parameters. $J_{1up}(HC_3N) \leq 15$ (10 for He). Methods: CC, Close coupling, CS, Coupled states approx., IOS, Infinite Order Sudden approx.

$\sigma_{J_1 J_1'}(E)$, HC_3N – para-H_2 collisions		
E_{tot} (cm^{-1})	Energy step (cm^{-1})	Method
$0.3 \rightarrow 60$	0.1	CC
$60 \rightarrow 110$	10	CC
$40 \rightarrow 200$	10	CS
$50 \rightarrow 800$	$10 - 100$	IOS
$\sigma_{J_1 J_1'}(E)$, HC_3N – ortho-H_2 collisions		
$0 \rightarrow 30$	1	CC
$\sigma_{J_1 J_1'}(E)$, HC_3N – He collisions		
$0 \rightarrow 25$	0.1	CC
$25 \rightarrow 100$	5	CC
$100 \rightarrow 150$	10	CC

formed quantum inelastic scattering calculations, as presented in next subsection 3.1. For $J_{1up} > 15$, we used the QCT method, as presented in subsection 3.2.

For He, of less astrophysical importance ([He]/[H]~ 0.1), only quantum calculations were performed and were limited to the low temperature regime (T=5−20 K and $J_1 < 10$).

3.1. Rotational inelastic cross sections with MOLSCAT

All calculations were made using the rigid rotor approximation, with rotational constants $B_{HC_3N} = 0.151739$ cm^{-1} and $B_{H_2} = 60.853$ cm^{-1}, using the MOLSCAT code (Hutson & Green 1994). All quantum calculations for HC_3N – ortho-H_2 were performed with $J_{H_2} \equiv J_2 = 1$. Calculations for HC_3N – para-H_2 were performed with $J_2 = 0$. We checked at $E_{tot} = E_{coll} + E_{rot} = 30$ cm^{-1} that the inclusion of the closed $J_2 = 2$ channel led to negligible effects.

The energy grid was adjusted to reproduce all the details of the resonances, as they are essential to calculate the rates with high confidence (Dubernet & Grosjean 2002; Grosjean et al. 2003; Wernli et al. 2006). The energy grid and the quantum methods used are detailed in table 1. Using this grid, we calculated the whole resonance structure of all the transitions up to $J_1 = 15$ for the HC_3N – para-H_2 collisions. At least 10 closed channels were included at each energy to fully converge the HC_3N rotational basis. We used the hybrid log-derivative/Airy propagator (Alexander & Manolopoulos 1987). We increased the parameter STEPS at the lowest energies to constrain the step length of the integrator below 0.1 to 0.2 Bohr, in order to properly follow the details of the radial coefficients. Other propagation parameters were taken as the MOLSCAT default values.

Two examples of deexcitation cross-sections are shown in figure 2. We see that for energies between threshold and about 20 cm^{-1} above threshold, the cross-section displays many shape resonances, justifying *a posteriori* our very fine energy grid. This behaviour is by no means unexpected and is very similar to most earlier calculations is many different systems, see e.g. Dubernet & Grosjean (2002); Wernli et al. (2006) for

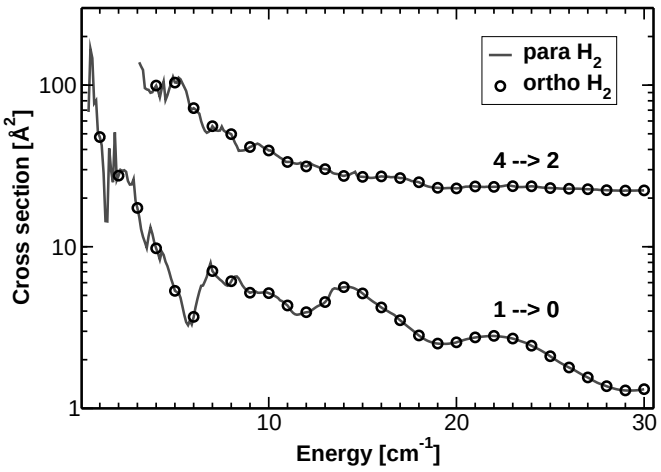

Fig. 2. $HC_3N - H_2$ collisions. Quantum deexcitation cross sections for transitions $J_1 = 1 \rightarrow 0$ (lower trace) and $J_1 = 4 \rightarrow 2$ (upper trace) as a function of the energy E=E_{coll} + $E_{rot(HC_3N)}$. Full line, para-H_2 ($J = 0$) collisions (0.1 cm^{-1} energy spacing); open circles, ortho-H_2 ($J = 1$). The fine energy grid emphasizes the resonances for $E \lesssim 10$ cm^{-1}.

a discussion. In a semi-classical point of view, those shape resonances manifest the trapping of the wave-packet between the inner repulsive wall and the outer centrifugal barrier, see Wiesenfeld et al. (2003); Abrol et al. (2001). At energies higher than about 20 cm^{-1} above threshold, all cross-sections become smooth functions of the energy.

Figure 2 also shows that ortho-H_2 inelastic cross-sections follow very closely the para-H_2 ones, including the position of resonances. Examination of all cross-sections reveals that the relative difference between $\sigma_{J_1 J_1'}(E, \text{para})$ and $\sigma_{J_1 J_1'}(E, \text{ortho})$ is less than 5%. This justifies *a posteriori* the much smaller amount of computational effort devoted to ortho-H_2 collisions as well as the neglect of $J_2 = 2$ closed para-H_2 channels. A detailed discussion of this behaviour is put forward in section 4.1.

3.2. Quantum rates and classical rates

The quantum collisional rates are calculated for $J_{1up} \leq 15$, at astrophysically relevant temperatures, from 5 K to 100 K. We average the cross-sections described in the preceding section over the Maxwell distribution of velocities, up to a kinetic energy at least 10 times kT. The quantum calculations at the higher end of the energy range are approximated at the IOS level (see table 1), which is justified at these energies by the smallness of the rotational constant B_{HC_3N}. Also we used a coarse energy grid for the IOS calculations because the energy dependence of the cross-sections becomes very smooth.

For values of $J_1 > 15$, the close coupling approach enters a complexity barrier due to the rapid increase of the number of channels involved in calculations, while memory and CPU requirements scale as the square and the cube of this number, respectively. Resorting to quantum CS or IOS approximations is inaccurate, because the energy is close to threshold for high-J_1 channels. In the meanwhile, the accuracy of classical ap-

proximations improves for higher collisional energies. For the energy range where $J_1 > 15$ channels are open *and* for deexcitation processes involving those channels, we employ a Quasi-Classical Trajectory (QCT) method, which has been shown at several instances to be a valid approximation for higher collisional energies and large rates (Chapman & Green 1977; Lepp et al. 1995; Mandy & Progrebnya 2004; Faure et al. 2006).

For Monte-Carlo QCT methods, we must devise a way of defining an ensemble of initial conditions for classical trajectories, on the one hand, and of analyzing the final state of each trajectory, on the other hand. Contrary to the asymmetric rotor case (like water, see Faure & Wiesenfeld 2004), the analysis of final conditions for a linear molecule is straightforward. Using the simplest quantization approximation, we bin the final classical angular momentum J'_1 of HC_3N to the nearest integer. While the quantum formalism goes through a microcanonical calculation —calculating $\sigma_{J_1 J'_1}(E)$ for fixed energies, then averaging over velocity distributions— it is possible for QCT calculations to directly resort to a canonical formalism, i.e. to select the initial velocities of the Monte-Carlo ensemble according to the relevant Maxwell-Boltzmann distribution and find the rates as:

$$k_{J_1 J'_1} = \left(\frac{8kT}{\pi\mu}\right)^{1/2} \pi b_{max}^2 \frac{N}{N_{\rm tot}} \tag{3}$$

where b_{max} is the maximum impact parameter used (with the impact parameter b distributed with the relevant $b\,\mathrm{d}b$ probability density) and N is the number of trajectories with the right final J'_1 value among all $N_{\rm tot}$ trajectories. The Monte-Carlo standard deviation is:

$$\frac{\delta k_{J_1 J'_1}}{k_{J_1 J'_1}} = \left(\frac{N_{\rm tot} - N}{N_{\rm tot} N}\right)^{1/2} \quad , \tag{4}$$

showing that the accuracy of the method improves for larger rates. The b_{max} parameter was determined by sending small batches of 500 to 1,000 trajectories for fixed b values; values of $20 \leq b_{max} \leq 26$ Bohr were found. We then sent batches of 10,000 trajectories for each temperature in the range 5 – 100K, with a step of 5K. Trajectories are integrated by means of a Bürlich-Stoer algorithm (Press et al. 1992), with a code similar to that of Faure et al. (2005b). Precision is checked by conservation of total energy and total angular momentum.

Some illustrative results are shown in tables 2 and 3 and are illustrated in figures 3 and 4.

As an alternative to QCT calculations, we tested J-extrapolation techniques, using the form of DePristo et al. (1979) generally used by astrophysicists (see for example Schöier et al. (2005), section 6). We found that even if it reproduces the interference pattern, the extrapolation systematically underestimates the rates, for $J_1 \geq 20$. Hence, QCT rates are more precise in the average.

For H_2, all deexcitation rates $k_{J_1 J'_1}(T)$, $J_1 \neq J'_1 \leq 50$, are fitted with the following formula (Wernli et al. 2006):

$$\log_{10}\left(k_{J_1 J'_1}(T)\right) = \sum_{n=0}^{4} a^{(n)}_{J_1 J'_1} x^n \tag{5}$$

Table 2. HC_3N – para-H_2 s($J = 0$)collisions. Quantum deexcitation rates in $\mathrm{cm}^3\,\mathrm{s}^{-1}$, for $J'_1 = 0$, for successive initial J_1 and for various temperatures. Powers of ten are denoted in parenthesis.

J_1	T = 10K	T = 20K	T = 50K	T = 100K
1	2.03(-11)	1.59(-11)	1.32(-11)	1.24(-11)
2	4.94(-11)	4.83(-11)	6.23(-11)	8.04(-11)
3	1.20(-11)	1.04(-11)	8.23(-12)	7.43(-12)
4	2.25(-11)	2.57(-11)	2.85(-11)	2.87(-11)
5	7.01(-12)	6.80(-12)	5.62(-12)	4.77(-12)
6	9.15(-12)	1.18(-11)	1.42(-11)	1.38(-11)
7	3.14(-12)	3.40(-12)	3.46(-12)	3.26(-12)
8	2.45(-12)	3.71(-12)	5.92(-12)	6.61(-12)
9	1.63(-12)	1.63(-12)	1.95(-12)	2.18(-12)
10	5.35(-13)	8.13(-13)	2.00(-12)	2.96(-12)
11	7.81(-13)	7.01(-13)	9.42(-13)	1.36(-12)
12	1.37(-13)	1.58(-13)	6.17(-13)	1.32(-12)
13	2.74(-13)	2.51(-13)	4.17(-13)	8.26(-13)
14	4.14(-14)	4.65(-14)	2.24(-13)	6.28(-13)
15	7.63(-14)	8.26(-14)	1.76(-13)	4.85(-13)

where $x = T^{-1/6}$. As some transitions have zero probability within the QCT approach, the above formula was employed when rates were bigger than 10^{-12} $\mathrm{cm}^3\mathrm{s}^{-1}$ for at least one grid temperature. For these rates, null grid values were replaced by a very small value, namely 10^{-14} $\mathrm{cm}^3\mathrm{s}^{-1}$, to avoid fitting irregularities. All rates not fulfilling this condition are set to zero. Note that below 20 K, QCT rates for low-probability transitions may show a non physical behaviour. All $a^{(n)}_{J_1 J'_1}$ coefficients are provided as online material, for a temperature range $5\ \mathrm{K} \leq T \leq 100\ \mathrm{K}$. We advise to use the same rates for collisions with ortho-H_2 as for para-H_2, since their difference is smaller than the uncertainty on the rates themselves. Rates with He were not fitted, but can be obtained upon request to the authors.

4. Discussion

4.1. Para and ortho H_2 cross-sections

A comparison of the $\sigma_{J_1 J'_1}(E)$ cross sections for HC_3N with ortho-H_2 and para-H_2 is given in figure 2. It can be seen that the difference between the two spin species of H_2 may be considered as very small, in any case smaller than other PES and cross-section uncertainties. This is an unexpected result, as sizeable differences between para-H_2 and ortho-H_2 inelastic cross-sections exist for other molecules. These differences were expected to increase for a molecule possessing a large dipolar moment, in view of the results obtained for the C_2 molecule (Phillips 1994), the CO molecule (Wernli et al. 2006), the OH radical (Offer et al. 1994), the NH_3 molecule (Offer & Flower 1989; Flower & Offer 1994) and the H_2O molecule (Phillips et al. 1996; Dubernet & Grosjean 2002; Grosjean et al. 2003; Dubernet et al. 2006), due to the interaction between the dipole of the molecule and the quadrupole of H_2 ($J_2 > 0$).

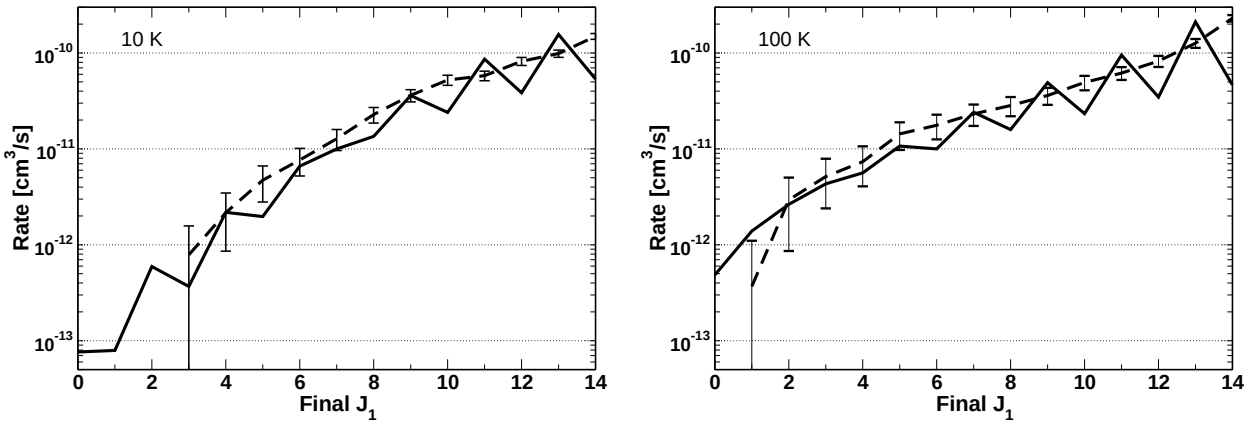

Fig. 4. HC_3N -para H_2 collisions. Deexcitation rates, from $J_1 = 15$, at 10 K (left panel) and 100 K (right panel). Full black line, lations with error bars.

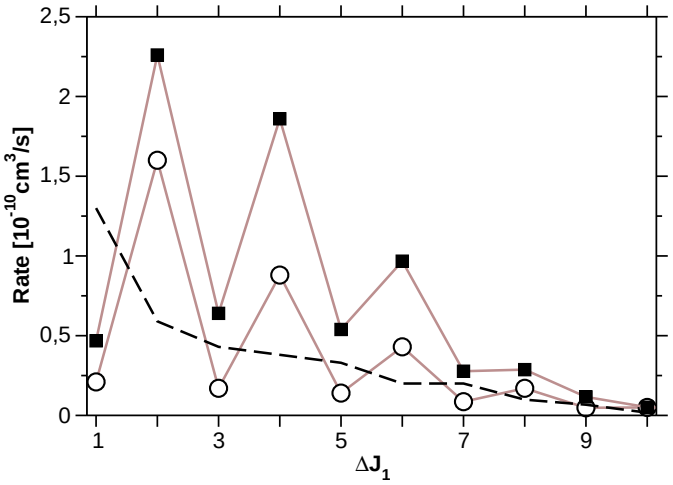

Fig. 3. Collisional excitation rates for HC_3N, from $J_1 = 0$, at 20 K. Present quantum close-coupling rates: Open circles, HC_3N – He collisions; filled squares, HC_3N – para-H_2 ($J = 0$). Gray lines serve as a guide to the eyes. For sake of comparison, QCT rates for the HC_3N – He (Green & Chapman 1978) are shown as dashed line.

This apparently null result deserves an explanation. We focus on equation (9) of Green (1975). This equation describes the different matrix elements that couple the various channels in the close-coupling equations. Some triangle rules apply which restrict the number of terms in the sum of equation (9); the relevant angular coupling algebra is represented there as a sum of terms of the type

$$\begin{pmatrix} l & L' & L \\ 0 & 0 & 0 \end{pmatrix} \begin{pmatrix} l_1 & J_1' & J_1 \\ 0 & 0 & 0 \end{pmatrix} \begin{pmatrix} l_2 & J_2' & J_2 \\ 0 & 0 & 0 \end{pmatrix} \begin{Bmatrix} L' & L & l \\ J_{12} & J_{12}' & J \end{Bmatrix} \quad , \qquad (6)$$

where we have the potential function expanded in terms of Eqs. (4) and (A2) in Green (1975), by means of the coefficients $v_{l_1 l_2 l}$. The symbol $(\ldots)$ are 3-j symbols, the $\{\ldots\}$ is a 6-j symbol, see Messiah (1969). We also define $\boldsymbol{J}_{12} = \boldsymbol{J}_1 + \boldsymbol{J}_2$. We have the following rules:

– The para-H_2 inelastic collisions are dominated by the $J_2 = 0$ channel (the $J_2 = 2$ channel is closed till $E_{coll} \gtrsim$ 365.12 cm^{-1}). Then, only the $l_2 = 0$ may be retained ($J_2 = J_2' = 0$), due to the third 3-j symbol in eq.(6).
– The ortho-H_2 remains in $J_2 = 1$, implying $l_2 = 0, 2$.
– For inelastic collisions, $J_1 \neq J_1'$ implies potential terms with $l \neq 0$, because of the 6-j term in Eq.(6). Indeed, $J_2 = J_2'$ and $J_1 \neq J_1'$ entail $J_{12} \neq J_{12}'$.

The key point is thus to compare the $v_{l_1 l_2 l}(R)$ coefficients (eq. 2) with $l \neq 0$ in the two cases:

– $l_2 = 0$ para and ortho contributions;
– $l_2 = 2$ ortho contribution only.

Figure 5 displays such a comparison. We notice that the coupling is largely dominated by the $l_2 = 0$ contribution, terms which are common to collisions with para and ortho conformations. This is particularly true for $R < 10$ Bohr, the relevant part of the interaction for collisions at temperatures higher than a few Kelvin. At a higher intermolecular separation, terms implied only in collisions with ortho-H_2 become dominant, but in this regime the potential is also less than a few cm^{-1}. Sizeable differences in rates between ortho and para forms are thus expected only either at very low temperatures, or possibly at much higher temperatures, with the opening of H_2 ($J_2 = 2, 3$) channels.

4.2. Propensity rules

In figure 3, we compare the various rates that we obtain here with the ones previously published by Green & Chapman (1978). These authors used a coarse electron-gas approximation for the PES, and computed rates by a QCT classical approach. Despite these approximations, we see that the rates obtained by Green & Chapman (1978) are qualitatively comparable with the quantum rates obtained here, in an average way. However, as table 3 and figures 4 and 3 show clearly, only quantum calculations manifest the strong $\Delta J = 2$ propensity rule. This rule originates in the shape of the PES, being nearly a prolate ellipsoid, dominated by the rod shape of HC_3N and *not dominated* by the large dipole of HC_3N molecule (3.724 Debye). Because of the very good approximate symmetry $\theta_1 \leftrightarrow \pi - \theta_1$, the l_1 even terms (equation (6)

Table 3. HC_3N – para-H_2 collisions. Quantum or QCT (†) de-excitation rates in $cm^3\,s^{-1}$, for $J_1 - J_1' = 1, 2, 3, 4$, for various temperatures and representative values of J_1. Powers of ten are denoted in parenthesis.

J_1'	J_1	T = 10K	T = 20K	T = 50K	T = 100K
0	1	2.03(-11)	1.59(-11)	1.32(-11)	1.24(-11)
0	2	4.94(-11)	4.83(-11)	6.23(-11)	8.04(-11)
0	3	1.20(-11)	1.04(-11)	8.23(-12)	7.43(-12)
0	4	2.25(-11)	2.57(-11)	2.85(-11)	2.87(-11)
5	6	6.34(-11)	5.48(-11)	4.80(-11)	4.64(-11)
5	7	1.30(-10)	1.38(-10)	1.72(-10)	2.04(-10)
5	8	3.93(-11)	3.66(-11)	3.27(-11)	3.21(-11)
5	9	6.83(-11)	7.61(-11)	8.63(-11)	8.93(-11)
10	11	5.77(-11)	5.35(-11)	4.75(-11)	4.61(-11)
10	12	1.50(-10)	1.53(-10)	1.81(-10)	2.11(-10)
10	13	3.91(-11)	3.80(-11)	3.50(-11)	3.40(-11)
10	14	8.51(-11)	8.84(-11)	9.42(-11)	9.47(-11)
15	16 †	1.45(-10)	1.49(-10)	1.80(-10)	2.28(-10)
15	17 †	1.06(-10)	1.03(-10)	9.60(-11)	1.18(-10)
15	18 †	8.71(-11)	9.38(-11)	7.93(-11)	8.24(-11)
15	19 †	7.59(-11)	6.81(-11)	6.23(-11)	7.10(-11)
25	26 †	1.14(-10)	1.50(-10)	1.83(-10)	2.30(-10)
25	27 †	1.13(-10)	1.05(-10)	1.18(-10)	1.31(-10)
25	28 †	8.55(-11)	8.38(-11)	8.34(-11)	7.76(-11)
25	29 †	7.67(-11)	7.45(-11)	8.31(-11)	7.02(-11)
35	36 †	1.16(-10)	1.34(-10)	1.73(-10)	2.32(-10)
35	37 †	9.63(-11)	1.12(-10)	1.21(-10)	1.11(-10)
35	38 †	8.33(-11)	9.20(-11)	8.56(-11)	9.19(-11)
35	39 †	8.77(-11)	8.51(-11)	7.65(-11)	7.51(-11)

and Green (1975)) are the most important ones, directing the inelastic transition toward even ΔJ_1. This propensity has also been explained semi-classically by McCurdy & Miller (1977) in terms of an interference effect related to the even anisotropy of the PES. These authors show in particular that the reverse propensity can also occur if the odd anisotropy of the PES is sufficiently large. This reverse effect is indeed observed in Fig. 4 for transitions with $\Delta J > 10$. A similar propensity rule has been experimentally observed for CO–He collisions (Carty et al. 2004).

Besides this strong $\Delta J = 2$ propensity rule, one can see from table 3 and figures 3, 4 that the rod-like interaction drives large ΔJ transfers. For instance, for T > 20 K, rates for $\Delta J > 6$ are generally larger than rates for $\Delta J = 1$, and rates for $\Delta J > 8$ are only one order of magnitude below those for $\Delta J = 2$. This behaviour is likely to emphasize the role of collisional effects versus radiative ones. This effect, of purely geometric origin, has been predicted previously (Bosanac 1980) and is of even greater importance for longer rods like HC_5N, HC_7N, HC_9N, see Snell et al. (1981); Bhattacharyya & Dickinson (1982).

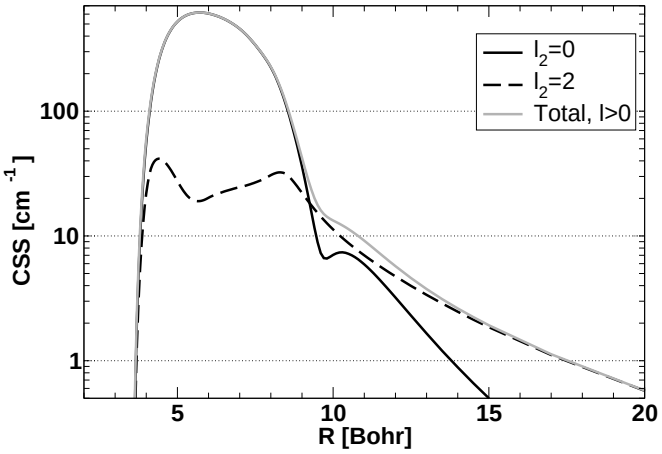

Fig. 5. Comparison of the coupling terms ($l \neq 0$) in the HC_3N – H_2 potential as a function of the intermolecular distance. CSS is $\left(\sum_{l\neq 0, l_1} v_{l_1 l_2 l}(R)^2\right)^{1/2}$. Terms with $l_2 = 0$ are common to ortho and para H_2, while the $l_2 = 2$ curve represents purely ortho terms. See text.

We also observe that the ratio $k_{J_1 J_1'}(\mathrm{He})/k_{J_1 J_1'}(\text{para-}H_2)$ is in average close to $1/1.4 \sim 1/\sqrt{2}$, thus confirming the similarity of He and para-H_2 as projectiles, as generally assumed. But it is also far from being a constant, as already observed for H_2O (Phillips et al. 1996) or CO (Wernli et al. 2006). Our data shows that the $1/\sqrt{2}$ scaling rule results in errors up to 50%.

4.3. Population inversion and critical densities

Because of the strong $\Delta J_1 = 0, 2, 4$ propensity rule, population inversion could be strengthened if LTE conditions are not met, even neglecting hyperfine effects[1] (Hunt et al. 1999). In order to see the density conditions giving rise to population inversion, we solved the steady-state equations for the population of the $J = 0, 1, \ldots, 15$ levels of HC_3N, including collisions with H_2 (densities ranging from 10^2 to 10^6 cm^{-3}), a black-body photon bath at 2.7 K, in the optically thin approximation, (Goldsmith 1972) :

$$\frac{\mathrm{d}n_i}{\mathrm{d}t} = 0 \;=\; +\sum_{j\neq i} n_j \left[A_{ji} + B_{ji}\, n_\gamma\left(\nu_{ji}\right) + k_{ji}\, n_{\mathrm{H_2}}\right] - n_i \sum_{j\neq i}\left[A_{ij} + B_{ij}\, n_\gamma\left(\nu_{ij}\right) + k_{ij}\, n_{\mathrm{H_2}}\right] \quad (7)$$

where i, j are the levels, n_γ is the photon density at temperature T_γ and $n_{\mathrm{H_2}}$ is the hydrogen density at kinetic temperature $T_{\mathrm{H_2}}$. Figure 6 shows the results at $T_{\mathrm{H_2}} = 40$ K. The lines show the population per sub-levels $\left|J_1, m_{J_1}\right\rangle$. For a consequent range of H_2 densities, $10^4 \lesssim n_{\mathrm{H_2}} \lesssim 10^6$, population inversion does occur, for $0 \leq J_1 \leq 2, 3, 4$. Our new rates are expected to improve the interpretation of the lowest-lying lines of HC_3N, especially so in the 9 - 20 GHz regions (cm-mm waves), see for example

[1] Hyperfine effects in HC_3N inelastic collisions will be dealt with in a forthcoming paper, Wiesenfeld et al. (2006)

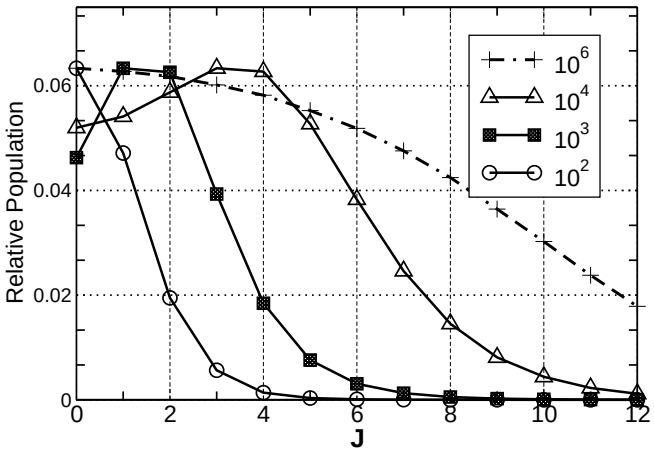

Fig. 6. Population per J_1, m_{J_1}-sub-level, following equation (7), for varying H_2 densities (in cm^{-3}) at a kinetic temperature of 40K.

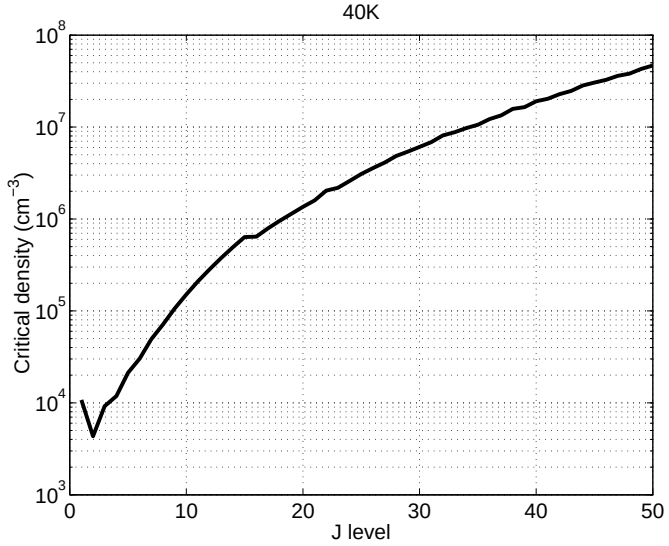

Fig. 7. H_2 critical density $n^\star$ (in cm^{-3}) for the HC_3N – para-H_2 collisions, at $T = 40$ K, equation (8). For $j \leq 15$, quantum rates, for $j > 15$, classical rates. The change of method explains the small discontinuity between $j = 15, 16$. The increase of critical density at $j = 1$ is related to the propensity rule, see figure 4.

Walmsley et al. (1986); Takano et al. (1998); Hunt et al. (1999), and Kalenskii et al. (2004) for a recent study. Moreover, from the knowledge of both collision coefficients k_{ij} and Einstein coefficients A_{ij}, it is possible to derive a critical density of H_2 , defined as:

$$n_i^\star(T) = \frac{\sum_{j<i} A_{ij}}{\sum_{j<i} k_{ij}} \tag{8}$$

The $n^\star$ density is the H_2 density at which photon deexcitation and collisional deexcitation are equal. The evolution of $n^\star$ with J_1 at $T = 40$ K is given in figure 7. It can be seen that for many common interstellar media, the LTE conditions are not fully met.

It must be underlined that similar effects should appear for the whole cyanopolyyne ($HC_{5,7,9}N$) family, where cross-sections should scale approximately with the rod length (Bhattacharyya & Dickinson 1982). It is expected that the propensity rule $\Delta J_1 = 2, 4, \ldots$ should remain valid. Also, the critical density should decrease for the higher members of the cyanopolyyne family, as the Einstein A_{ij} coefficients, hence facilitating the LTE conditions.

5. Conclusion

We have computed two *ab initio* surfaces, for the HC_3N – He and HC_3N – H_2 systems. The latter was built using a carefully selected set of H_2 orientations, limiting the computational effort to approximately five times the HC_3N – He one. Both surfaces were successfully expanded on a rotational basis suitable for quantum calculations using a smooth regularization of the potentials. This approach circumvented the severe convergence problems already noticed by Chapman & Green (1977) for such large molecules. The final accuracy of both PES is a few cm^{-1} for potential energy below 1000 cm^{-1}.

Rates for rotational excitation of HC_3N by collisions with He atoms and H_2 molecules were computed for kinetic temperatures in the range 5 to 20 K and 5 to 100 K, respectively, combining quantum close coupling and quasi-classical calculations. The rod-like symmetry of the PES strongly favours even ΔJ_1 transfers and efficiently drives large ΔJ_1 transfers. Quasi classical calculations are in excellent agreement with close coupling quantum calculations but do not account for the even ΔJ_1 interferences. For He, results compare fairly with Green & Chapman (1978) QCT rates, indicating a weak dependance to the details of the PES. For para-H_2, rates are compatible in average with the generally assumed $\sqrt{2}$ scaling rule, with a spread of about 50 %. Despite the large dipole moment of HC_3N, rates involving ortho-H_2 are very similar to those involving para-H_2, due to the predominance of the rod interactions.

A simple steady-state population model shows population inversions for the lowest HC_3N levels at H_2 densities in the range 10^4–10^6 cm^{-3}. This inversion pattern manifests the importance of large angular momentum transfer, and is enhanced by the even ΔJ_1 quantum propensity rule.

The HC_3N molecule is large enough to present an original collisional behaviour, where steric hindrance effects hide the details of the interaction, and where quasi classical rate calculations achieve a fair accuracy even at low temperatures. With these findings, approximate studies for large and heavy molecules should become feasible including possibly the modelling of large ΔJ transfer collisions and ro-vibrational excitation of low energy bending or floppy modes.

Acknowledgements. This research was supported by the CNRS national program "Physique et Chimie du Milieu Interstellaire" and the "Centre National d'Etudes Spatiales". LW was partly supported by a CNRS/NSF contract. MW was supported by the Ministère de l'Enseignement Supérieur et de la Recherche. CCSD(T) calculations were performed on the IDRIS and CINES French national computing centers (projects no. 051141 and x2005 04 20820). MOLSCAT and QCT calculations were performed on local workstations and on the

"Service Commun de Calcul Intensif de l'Observatoire de Grenoble" (SCCI) with the valuable help from F. Roch.

References

Abrol, R., Wiesenfeld, L., Lambert, B., & Kuppermann, A. 2001, J. Chem. Phys., 114

Akin-Ojo, O., Bukowski, R., & Szalewicz, K. 2003, J. Chem. Phys., 119, 8379

Alexander, M. H. & Manolopoulos, D. E. 1987, J. Chem. Phys., 86, 2044

Audinos, P., Kahane, C., & Lucas, R. 1994, A&A, 287, L5

Bell, M. B., Feldman, P. A., Travers, M. J., et al. 1997, ApJ, 483, L61+

Bell, M. B. & Matthews, H. E. 1985, ApJ, 291, L63

Bhattacharyya, S. S. & Dickinson, A. S. 1982, A&A, 107, 26

Bockelée-Morvan, D., Lis, D. C., Wink, J. E., et al. 2000, A&A, 353, 1101

Bosanac, S. 1980, Phys. Rev. A, 22, 2617

Boys, S. & Bernardi, F. 1970, Mol. Phys., 19, 553

Carty, D., Goddard, A., Sims, I. R., & Smith, I. W. M. 2004, J. Chem. Phys., 121, 4671

Caux, E. 2006, private communication.

Chapman, S. & Green, S. 1977, J. Chem. Phys., 67, 2317

DePristo, A. E., Augustin, S. D., Ramaswamy, R., & Rabitz, H. 1979, J. Chem. Phys., 71, 850

Dubernet, M.-L., Daniel, F., Grosjean, A., et al. 2006, in print.

Dubernet, M.-L. & Grosjean, A. 2002, A&A, 390, 793

Faure, A., Valiron, P., Wernli, M., et al. 2005a, J. Chem. Phys., 122, 1102

Faure, A. & Wiesenfeld, L. 2004, J. Chem. Phys., 121, 6771

Faure, A., Wiesenfeld, L., Wernli, M., & Valiron, P. 2005b, J. Chem. Phys., 123, 104309

Faure, A., Wiesenfeld, L., Wernli, M., & Valiron, P. 2006, J. Chem. Phys., 124, 214310

Flower, D. R. & Offer, A. 1994, in AIP Conf. Proc. 312: Molecules and Grains in Space, ed. I. Nenner, 477–+

Goldsmith, P. F. 1972, ApJ, 176, 597

Gordy, W. & Cook, R. L. 1984, Microwave Molecular Spectra (New York: Wiley)

Green, S. 1975, J. Chem. Phys., 62, 2271

Green, S. & Chapman, S. 1978, ApJS, 37, 169

Grosjean, A., Dubernet, M.-L., & Ceccarelli, C. 2003, A&A, 408, 1197

Hodges, M. P., Wheatley, R. J., Schenter, G. K., & Harvey, A. H. 2004, J. Chem. Phys., 120, 710

Hunt, M. R., Whiteoak, J. B., Cragg, D. M., White, G. L., & Jones, P. A. 1999, MNRAS, 302, 1

Hutson, J. M. & Green, S. 1994, MOLSCAT computer code, version 14 (1994) (distributed by Collaborative Computational Project No. 6 of the Engineering and Physical Sciences Re search Council UK)

Jankowski, P. & Szalewicz, K. 2005, J. Chem. Phys., 123, 4301

Jansen, H. & Ross, P. 1969, Chem. Phys. Lett., 3, 140

Jeziorska, M., Jankowski, P., Szalewicz, K., & Jeziorski, B. 2000, J. Chem. Phys., 113, 2957

Kalenskii, S. V., Slysh, V. I., Goldsmith, P. F., & Johansson, L. E. B. 2004, ApJ, 610, 329

Kuan, Y.-J., Huang, H.-C., Charnley, S. B., et al. 2004, ApJ, 616, L27

Kunde, V. G., Aikin, A. C., Hanel, R. A., et al. 1981, Nature, 292, 686

Lepp, S., Buch, V., & Dalgarno, A. 1995, ApJS, 98, 345

Mandy, S. E. & Progrebnya, S. 2004, J. Chem. Phys., 120, 5584

Mauersberger, R., Henkel, C., & Sage, L. J. 1990, A&A, 236, 63

McCurdy, C. W. & Miller, W. H. 1977, J. Chem. Phys., 67, 463

Messiah, A. 1969, Mécanique Quantique, Vol. 2 (Paris: Dunod)

Noga, J., Valiron, P., Klopper, W., & Helgaker, T. 2003-2006, direct CC-R12 program repository on: http://www-laog.obs.ujf-grenoble.fr/~valiron/ccr12/index.html

Offer, A. & Flower, D. R. 1989, Journal of Physics B Atomic Molecular Physics, 22, L439

Offer, A. R., van Hemert, M. C., & van Dishoeck, E. F. 1994, J. Chem. Phys., 100, 362

Pardo, J. R., Cernicharo, J., Goicoechea, J. R., & Phillips, T. G. 2004, ApJ, 615, 495

Phillips, T. R. 1994, MNRAS, 271, 827

Phillips, T. R., Maluendes, S., & Green, S. 1996, ApJS, 107, 467

Press, W., Teukolsky, S., Vetterling, W., & Flannery, B. 1992, Numerical Recipes in Fortran, 2nd edn. (Cambridge University Press)

Schöier, F. L., van der Tak, F. F. S., van Dishoeck, E. F., & Black, J. H. 2005, A&A, 432, 369

Snell, R. L., Schloerb, F. P., Young, J. S., Hjalmarson, A., & Friberg, P. 1981, ApJ, 244, 45

Takano, S., Masuda, A., Hirahara, Y., et al. 1998, A&A, 329, 1156

Thorwirth, S., Müller, H., & Winnewisser, G. 2000, J. Mol. Spec., 204, 133

Topic, W. C. & Wolfgang, J. 2005, J. Chem. Phys., 123, 064303

Walmsley, C. M., Guesten, R., Angerhofer, P., Churchwell, E., & Mundy, L. 1986, A&A, 155, 129

Wernli, M. 2006, Thèse de Doctorat, spécialité Astrophysique - Université Joseph Fourier, Grenoble 1

Wernli, M., Valiron, P., Faure, A., et al. 2006, A&A, 446, 367

Wiesenfeld, L., Faure, A., & Johann, T. 2003, J. Phys. B, At. Mol. Opt. Phys., 36, 1319

Wiesenfeld, L., Requena Torres, M., Morris, M., et al. 2006, in preparation

Wyrowski, F., Schilke, P., Thorwirth, S., Menten, K. M., & Winnewisser, G. 2003, ApJ, 586, 344

Table A1. Fitting coefficients of HC_3N-para-H_2(J_2=0) rates, following formula (5). J_1 and J_1' are the initial and final rotation states, respectively. The rates thus obtained are in cm^3s^{-1}. Rates are quantum for $J_{1up} \leq 15$, classical otherwise

J_1	J_1'	$a^{(0)}$	$a^{(1)}$	$a^{(2)}$	$a^{(3)}$	$a^{(4)}$
1	0	-25.51832	106.88002	-291.58814	350.10316	-154.84199
2	0	-24.35512	106.84051	-287.22039	328.93070	-136.65661
2	1	-14.61936	33.10754	-100.86405	134.46313	-64.92410
3	0	-5.47571	-35.76987	79.22847	-71.33148	21.84669
3	1	-14.72047	37.31354	-99.10777	109.36028	-43.08167
3	2	-10.28982	0.65318	-9.29094	22.34848	-14.56401
4	0	-7.41774	-26.73297	82.55022	-109.01113	51.70164
4	1	-3.38680	-51.59920	129.83555	-139.00247	54.24922
4	2	-15.21990	38.99699	-97.70381	101.86978	-37.80211
4	3	-12.58261	16.11524	-46.07311	59.69880	-28.32805
5	0	-2.57002	-65.02497	173.34352	-196.93477	81.38532
5	1	-6.70478	-32.22515	104.01102	-141.22086	68.20796
5	2	-7.77688	-20.41374	51.00900	-52.23946	18.89396
5	3	-14.68567	35.11227	-86.12083	86.29616	-30.00840
5	4	-16.11594	42.59701	-118.20463	145.03851	-65.46450
6	0	-6.13685	-45.36061	149.75974	-205.86434	100.21101
6	1	-8.64971	-19.59865	56.44070	-66.00344	27.12532
6	2	-10.28772	-6.27935	36.89117	-65.85667	37.18314
6	3	-9.22466	-8.43687	17.48400	-12.41144	1.57029
6	4	-15.64671	43.10487	-109.73894	116.17416	-43.72905
6	5	-14.41336	32.47142	-95.78570	123.12942	-57.48288
7	0	-10.78341	-11.00360	42.71396	-62.38185	30.99555
7	1	-8.47134	-26.73320	103.12673	-156.24676	81.04140
7	2	-10.52514	-4.01783	14.11252	-17.79053	7.37242
7	3	-12.46550	11.17004	-13.17720	-3.74494	8.97429
7	4	-11.11202	7.70446	-30.98603	49.78866	-27.50257
7	5	-14.11456	32.83262	-84.04719	87.74861	-31.92234
7	6	-12.88796	23.22698	-75.25517	103.35455	-50.51406
8	0	-13.38837	0.02904	45.02589	-106.11757	66.91335
8	1	-16.15190	32.15754	-74.52365	74.52728	-27.21444
8	2	-12.41248	4.26702	16.28624	-50.87715	34.08956
8	3	-9.57815	-6.79964	13.57592	-9.78042	1.47624
8	4	-11.37909	4.75157	0.91307	-17.25883	13.85036
8	5	-8.91813	-5.80461	0.00434	18.44041	-15.62564
8	6	-18.13303	61.83878	-162.03735	180.33365	-72.79000
8	7	-9.90163	2.74864	-23.17369	45.17610	-26.51891
9	0	-29.82574	126.14490	-320.70118	353.45960	-143.05848
9	1	-16.43119	25.24029	-21.82079	-31.50924	36.98088
9	2	-18.13932	52.53034	-140.54421	163.21878	-69.81489
9	3	-11.60134	0.93022	19.76559	-49.25968	31.21266
9	4	-7.10154	-21.85393	47.93692	-44.39906	14.48424
9	5	-10.93830	2.33916	5.51949	-20.60739	14.54558
9	6	-5.02685	-32.82491	70.20632	-62.34203	19.12060
9	7	-14.24666	34.75272	-91.84970	100.19874	-38.71027
9	8	-7.79979	-12.45038	17.57024	-2.84443	-5.50013
10	0	-30.74777	114.05664	-225.51866	159.18442	-22.70276
10	1	-39.00410	200.75846	-532.95664	614.99802	-261.48335
10	2	-20.07566	54.80765	-106.43261	72.62945	-9.70628
10	3	-11.92876	11.94117	-40.44338	53.65904	-24.88768
10	4	-11.48476	1.42081	15.41256	-40.84799	26.37924
10	5	-3.85593	-43.46421	101.73389	-103.45405	38.59973
10	6	-11.31632	5.13387	-2.08303	-11.54640	10.66508

10	7	-3.67891	-43.12965	99.45931	-98.69278	35.76283
10	8	-13.90765	32.55352	-86.78912	95.40806	-37.14244
10	9	-6.60948	-21.44139	42.44674	-32.69685	7.57630
11	0	-69.08122	420.33417	-1134.19665	1332.58368	-577.17783
11	1	-40.26915	186.66520	-420.43692	385.05400	-118.45036
11	2	-37.90099	199.69566	-543.57701	640.21840	-276.73796
11	3	-20.14212	57.23802	-117.06233	89.62936	-18.81605
11	4	-9.67380	-0.68862	-15.15065	33.12554	-19.54264
11	5	-10.03000	-8.79385	42.23006	-71.83318	39.81500
11	6	-2.01512	-55.97720	133.45404	-138.83443	53.27885
11	7	-11.89745	9.29782	-13.14465	1.40714	5.11882
11	8	-3.52867	-44.91918	105.98087	-108.06217	40.38518
11	9	-16.98632	54.81510	-146.87723	167.18816	-69.11154
11	10	-6.27560	-24.43393	51.55426	-44.02788	12.42472
12	0	-110.08999	671.89795	-1673.39792	1794.52580	-702.20758
12	1	-79.23534	502.83570	-1369.45426	1623.10507	-709.17840
12	2	-43.96236	217.92588	-514.17089	506.98652	-176.78861
12	3	-31.26580	155.56616	-432.99781	517.61009	-226.10646
12	4	-15.66040	26.43792	-38.38127	1.62187	17.68910
12	5	-1.69568	-57.81035	137.41382	-146.62275	59.33281
12	6	-11.49393	1.85124	13.25291	-36.70366	23.97437
12	7	-1.30588	-61.40897	148.81232	-157.61190	61.64585
12	8	-13.30200	19.28527	-39.60948	32.39554	-8.32782
12	9	-3.93283	-42.70787	101.73134	-104.66734	39.48733
12	10	-14.58397	37.83552	-102.22653	115.34221	-46.61063
12	11	-6.84937	-20.88700	43.27719	-35.20778	8.76813
13	1	-121.42176	760.23690	-1919.78115	2095.24554	-838.35388
13	2	-73.43881	466.18432	-1280.50008	1526.86938	-670.24329
13	3	-37.46863	173.69762	-402.14277	383.07082	-126.22192
13	4	-25.11786	113.32185	-324.75123	395.89658	-175.53626
13	5	-16.31200	31.34417	-52.45879	20.16637	8.53283
13	6	-5.03111	-34.19360	74.82450	-72.55575	26.24645
13	7	-12.26751	7.51849	-2.38408	-17.31497	14.98484
13	8	-1.77878	-58.36783	141.41142	-149.22379	57.81292
13	9	-14.07839	25.17746	-56.25427	53.14293	-17.88514
13	10	-5.10621	-35.30788	84.48831	-86.84162	32.48677
13	11	-15.68430	45.37443	-121.47165	137.06234	-55.70906
13	12	-7.63435	-15.76136	30.71303	-21.37272	2.94020
14	1	-117.52398	791.58601	-2171.95252	2593.52489	-1142.29451
14	2	-101.97192	622.81734	-1556.51667	1672.17066	-655.34871
14	3	-64.97054	407.56112	-1127.80646	1350.92195	-594.71729
14	4	-33.40083	146.10829	-333.38038	309.34404	-97.51001
14	5	-22.24962	93.16380	-272.14826	336.05107	-150.44281
14	6	-15.97667	29.69922	-50.66280	22.10118	5.65358
14	7	-5.12027	-33.46409	72.46275	-68.78901	23.94264
14	8	-13.51141	16.62484	-27.36720	13.21097	1.11568
14	9	-2.85727	-51.51845	125.40322	-132.75179	51.47909
14	10	-14.81190	30.52822	-70.95472	71.18866	-26.15235
14	11	-6.25020	-27.64004	65.46158	-66.06082	24.03841
14	12	-16.86546	54.18749	-146.19281	167.84696	-69.99618
14	13	-9.39251	-3.93229	1.12685	11.39170	-10.73118
15	1	-187.76520	1243.63911	-3227.93849	3646.24535	-1519.57337
15	2	-112.58143	761.87334	-2104.01237	2525.18121	-1116.95420
15	3	-91.55082	548.48401	-1358.90665	1441.31923	-555.11323
15	4	-58.16941	359.46429	-1000.87810	1203.64034	-531.23265
15	5	-32.30239	138.91568	-316.64601	293.68577	-92.56396
15	6	-21.24176	85.02826	-248.35224	306.26621	-136.65828

15	7	-18.24773	46.22364	-95.83431	77.23616	-19.43065
15	8	-3.51225	-45.76402	106.93734	-110.49496	42.36352
15	9	-14.62984	24.72653	-49.48991	40.26732	-11.24332
15	10	-4.90746	-38.05020	92.52413	-97.23545	37.19573
15	11	-15.83536	37.88336	-90.78815	94.98344	-36.82878
15	12	-6.63674	-25.75461	62.34128	-63.76717	23.19492
15	13	-19.26132	71.66204	-193.76205	225.08345	-95.66104
15	14	-8.52544	-10.93663	21.95643	-15.56076	2.01564
16	1	2073.89337	-14655.06952	38446.56275	-44649.89192	19359.13030
16	2	-698.15542	4823.68370	-12519.96132	14235.30139	-5999.43022
16	3	-1266.41777	9036.67298	-24241.43039	28724.19981	-12697.95692
16	4	-458.51447	3197.51847	-8512.88000	10008.91118	-4392.75851
16	5	274.00544	-2014.02376	5304.88427	-6174.06457	2676.35074
16	6	-14.27306	106.95039	-489.92832	798.35342	-440.60154
16	7	-264.91830	1823.39524	-4860.10567	5706.44129	-2492.81571
16	8	-36.31032	158.17019	-353.45048	335.77150	-113.16458
16	9	79.93056	-643.90150	1711.67152	-2012.44228	881.86193
16	10	-84.44641	531.88147	-1422.48660	1679.31253	-738.82137
16	11	-46.42216	260.12543	-697.05290	823.92074	-362.77668
16	12	-82.79534	524.16306	-1406.20954	1661.91042	-730.39693
16	13	18.93955	-221.71427	630.59099	-790.38109	367.95194
16	14	60.59096	-503.09882	1338.49056	-1574.75274	691.15235
16	15	-74.88622	478.79648	-1301.57719	1553.58472	-688.35113
17	2	117.37789	-505.38058	347.20929	608.39922	-652.81492
17	3	-1371.02786	9920.79652	-26817.34279	31830.11048	-14017.67612
17	4	-206.21826	1347.69601	-3458.46579	3914.95462	-1665.40935
17	5	-283.06486	1853.18922	-4653.51988	5097.50760	-2058.91887
17	6	92.82350	-756.42502	2068.08084	-2509.26625	1135.05563
17	7	-24.19152	102.13131	-274.22996	309.78787	-127.16171
17	8	-271.23783	1812.13791	-4690.41209	5358.38195	-2283.01426
17	9	51.11578	-459.96725	1273.07267	-1551.30815	701.34767
17	10	8.48732	-125.23408	307.19333	-332.08725	133.16815
17	11	-57.43650	331.30479	-872.70994	1018.48718	-444.17876
17	12	113.69137	-881.39318	2332.98179	-2726.42447	1187.39902
17	13	-96.42097	615.29675	-1634.82029	1916.29144	-836.11570
17	14	184.53257	-1376.95394	3631.21874	-4231.07672	1838.23260
17	15	20.14809	-191.93225	455.02942	-475.94319	185.37764
17	16	-75.49937	469.40668	-1241.05521	1443.23465	-624.27240
18	4	-1062.05521	7552.66023	-20110.91574	23508.76040	-10197.46234
18	5	152.79431	-1489.28772	4884.13036	-6896.68249	3541.54426
18	6	241.60328	-1756.63875	4569.19000	-5270.90135	2269.97895
18	7	235.46868	-1776.08490	4789.99335	-5723.93297	2551.01675
18	8	-343.69880	2340.84398	-6117.97626	7042.40497	-3014.72475
18	9	88.11381	-756.92330	2149.19487	-2680.84646	1238.28533
18	10	122.80049	-940.30288	2473.30625	-2877.67706	1248.79905
18	11	84.51405	-673.65071	1776.61370	-2066.10155	893.79866
18	12	97.57784	-773.84537	2066.23602	-2436.21315	1070.14202
18	13	-134.89406	874.11969	-2288.04235	2648.81475	-1144.52168
18	14	171.93020	-1289.03959	3401.63219	-3967.11789	1725.41911
18	15	-90.68065	593.07025	-1622.80060	1956.74348	-877.14293
18	16	-50.19982	301.75703	-837.77739	1021.62923	-462.14167
18	17	6.02542	-104.95067	267.85159	-309.14692	134.87592
19	4	-1068.11296	7460.15389	-19543.17053	22507.76781	-9630.71099
19	5	-361.88593	2550.94200	-6805.67359	7892.26822	-3373.92306
19	6	-336.19081	2658.16220	-7951.65745	10355.75647	-4979.29469
19	7	-241.79058	1700.60986	-4649.25589	5588.93407	-2498.45652
19	8	-298.59733	1971.73342	-5028.45576	5659.10849	-2376.89343

19	9	258.53018	-1930.50715	5155.06224	-6075.76791	2663.43620
19	10	126.54378	-1004.43059	2743.07766	-3312.48892	1490.63371
19	11	-119.49514	754.44028	-1952.43954	2237.91604	-959.50920
19	12	-62.65451	349.28128	-876.97857	978.15593	-408.93286
19	13	169.82736	-1272.09194	3346.33721	-3888.84402	1684.86657
19	14	10.03155	-133.84773	327.03338	-351.04088	139.62640
19	15	-36.52434	195.28543	-534.39455	639.44170	-282.24329
19	16	1.15577	-85.44081	240.77925	-298.28997	137.17470
19	17	-52.91035	311.89785	-841.01323	998.65753	-440.90458
19	18	6.30942	-97.89757	222.90917	-223.06526	81.60545
20	5	-1092.86958	8133.95666	-22597.56110	27489.60234	-12378.73735
20	6	-690.14356	4645.43353	-11731.48176	12948.88675	-5283.21228
20	7	-462.67518	3154.66150	-8175.98034	9311.95613	-3939.34593
20	8	252.09771	-1873.73823	4996.11835	-5910.61245	2611.60398
20	9	-513.40952	3649.04932	-9860.89874	11754.11974	-5218.80027
20	10	11.22683	-139.01688	339.49461	-382.58804	165.65485
20	11	-160.61722	1043.39775	-2705.73394	3098.23161	-1322.94571
20	12	151.69809	-1171.17152	3147.47088	-3733.61062	1649.11198
20	13	179.94541	-1355.43399	3598.71801	-4224.11854	1849.16748
20	14	64.44229	-535.41079	1425.43443	-1673.53297	731.06078
20	15	67.04543	-555.65363	1490.42556	-1768.63994	783.39552
20	16	-126.72327	819.22237	-2146.79511	2485.86313	-1073.17499
20	17	-131.45472	878.54495	-2367.70258	2815.41424	-1246.17098
20	18	20.34383	-211.62099	550.89903	-633.28077	271.00912
20	19	106.32388	-820.78536	2168.18463	-2533.17780	1103.24490
21	6	-396.04084	2707.31199	-7008.80423	7900.63877	-3284.43982
21	7	-797.94902	5568.10111	-14603.90154	16815.74936	-7188.20217
21	8	104.02906	-1111.00043	3794.26444	-5514.66816	2891.02772
21	9	-379.22779	2711.09012	-7421.05783	8953.72254	-4024.63727
21	10	106.97020	-863.24346	2374.84030	-2905.79721	1329.29051
21	11	-295.50438	2091.84461	-5699.40433	6826.53646	-3036.01147
21	12	36.09375	-313.58721	790.63293	-888.23900	373.80363
21	13	-125.42563	839.01699	-2283.11585	2741.93844	-1226.55106
21	14	132.65392	-1012.98000	2669.47442	-3104.05929	1343.69910
21	15	-65.33903	384.06044	-999.77924	1148.73484	-491.33493
21	16	-60.20245	331.77670	-819.24991	890.04860	-358.49283
21	17	74.78889	-597.83982	1568.02567	-1817.08191	785.11873
21	18	101.27811	-796.48686	2124.27212	-2504.02792	1100.95205
21	19	2.29053	-88.32898	237.36292	-280.67821	122.95873
21	20	2.62265	-66.49764	127.28807	-97.77772	21.54784
22	7	-3408.65715	24143.70871	-63840.23361	74429.78838	-32301.22363
22	8	1263.84082	-8934.94142	23331.65979	-26917.35666	11566.92278
22	9	-349.94892	2665.41053	-7773.47899	9970.69104	-4756.90347
22	10	-111.57437	719.54792	-1900.83467	2203.83721	-953.85518
22	11	-277.87411	1906.72551	-5070.17528	5950.58727	-2604.38441
22	12	-202.92832	1383.42614	-3708.16568	4387.72310	-1936.78971
22	13	-33.56219	169.35446	-462.80402	553.58919	-245.70905
22	14	-115.41636	746.41100	-1974.37838	2300.77194	-997.62768
22	15	-115.80405	737.83554	-1923.78241	2212.61970	-947.22469
22	16	-157.83215	1041.62821	-2741.91680	3188.56097	-1382.32448
22	17	-109.87652	702.50094	-1848.03780	2148.67780	-931.34544
22	18	45.21210	-412.89111	1145.02344	-1400.21172	637.23775
22	19	62.88926	-490.03654	1224.36560	-1349.37837	553.86363
22	20	-45.78281	259.18757	-695.41791	820.80369	-359.96111
22	21	-23.06715	116.11616	-357.59784	471.14033	-227.18411
23	8	-2181.44690	15698.24223	-42174.61732	49865.49134	-21912.21039
23	9	-257.04756	1651.31466	-4015.81237	4169.26525	-1561.57067

23	10	-266.89847	1779.33500	-4569.38398	5126.86687	-2124.06129
23	11	60.17208	-486.08132	1257.58797	-1462.24051	639.95616
23	12	-28.08944	81.03985	-102.05168	-17.90737	67.74493
23	13	219.45359	-1607.70732	4174.62923	-4777.44504	2031.30292
23	14	283.25877	-2071.73595	5452.25532	-6349.06385	2758.75798
23	15	-97.69814	645.27498	-1769.07041	2128.94829	-949.75642
23	16	-59.94507	357.67492	-960.23934	1135.05914	-498.58268
23	17	-93.01639	596.56628	-1604.77287	1905.98352	-843.01336
23	18	-49.88335	281.00993	-737.68586	849.50314	-362.01797
23	19	-19.73708	74.95899	-214.25977	266.84461	-122.56251
23	20	76.65441	-621.73962	1662.03988	-1962.86013	864.05955
23	21	-8.60437	-23.76177	103.56856	-170.11091	95.25838
23	22	81.44132	-640.60203	1682.99915	-1957.09361	848.68295
24	9	287.09907	-2134.67134	5776.32085	-7010.38333	3198.28258
24	10	-965.15204	6937.13835	-18745.67500	22310.11627	-9883.27294
24	11	-438.82019	3141.08710	-8556.66452	10249.58339	-4563.26429
24	12	-176.82153	1203.04512	-3229.27202	3801.01170	-1659.54477
24	13	154.51680	-1175.61601	3122.31963	-3669.90509	1606.73578
24	14	-108.73955	699.27717	-1851.32498	2156.18589	-934.32383
24	15	74.11457	-595.85477	1566.78428	-1826.19610	794.89197
24	16	-5.69208	-63.06908	248.29298	-390.58497	214.96346
24	17	147.77279	-1135.35191	3037.24619	-3590.20560	1582.29011
24	18	-86.34978	539.29630	-1425.78321	1664.66184	-724.05677
24	19	45.59527	-415.58438	1148.41714	-1397.28528	631.79950
24	20	-30.84298	144.90169	-376.19916	428.82513	-180.79960
24	21	-26.35735	115.17997	-301.31647	345.51761	-146.38722
24	22	-85.16701	540.69678	-1445.89907	1705.98521	-749.85166
24	23	68.32281	-543.64961	1416.77649	-1635.09544	703.88006
25	10	638.29214	-4806.40309	13295.88004	-16282.72737	7426.36872
25	11	-836.64186	6043.58082	-16463.20058	19785.15258	-8864.73409
25	12	1107.68668	-8044.12755	21585.23189	-25610.23116	11326.76210
25	13	-266.74355	1922.32996	-5367.74471	6604.22203	-3025.77152
25	14	259.31310	-1930.01145	5149.50397	-6079.44225	2676.38578
25	15	-120.17922	804.62041	-2194.59025	2633.92750	-1176.14654
25	16	-187.32932	1260.55438	-3347.39813	3922.53525	-1712.61168
25	17	-193.14446	1286.91156	-3371.93465	3893.47294	-1672.40309
25	18	-213.41217	1448.72957	-3854.90934	4531.59951	-1985.63135
25	19	-59.79251	341.52571	-878.47768	997.17011	-421.36557
25	20	-75.61264	462.68476	-1221.97673	1426.32639	-620.51037
25	21	-55.34024	324.25548	-867.09775	1023.57626	-449.96139
25	22	-16.19128	56.82749	-184.25486	253.45780	-126.29839
25	23	-0.96952	-60.47498	155.12556	-178.79422	77.67547
25	24	-32.14289	161.21904	-423.82433	485.43989	-206.04437
26	11	-1405.23905	10283.10272	-28090.87173	33678.15318	-14973.55704
26	12	-3248.27844	23173.78068	-61734.21020	72536.46270	-31736.19160
26	13	-549.23157	3923.78011	-10657.27870	12782.72138	-5719.67651
26	14	134.79971	-1027.23067	2719.22490	-3200.92568	1408.68268
26	15	222.62873	-1708.26580	4662.33079	-5623.17605	2524.84753
26	16	-8.77975	8.69760	-73.24710	132.09810	-73.50787
26	17	106.21876	-847.24631	2288.60623	-2727.20561	1208.07221
26	18	-119.93128	788.01462	-2117.48946	2514.92121	-1113.90203
26	19	-27.83557	102.31978	-214.90235	185.65781	-52.20188
26	20	-64.04422	389.27403	-1052.85157	1258.17649	-560.01890
26	21	-47.99006	253.13154	-636.20785	710.43691	-297.37773
26	22	205.69382	-1539.18183	4088.07797	-4794.15003	2094.88228
26	23	48.65873	-410.63236	1072.51022	-1240.85610	536.88911
26	24	-38.59269	206.57014	-552.02693	648.63325	-283.05731

26	25	-78.23440	505.20920	-1380.44742	1659.84965	-742.87462
27	12	109.65883	-985.87924	3026.08619	-4116.51833	2066.57988
27	13	317.59053	-2516.71923	7218.29146	-9171.17454	4335.04781
27	14	-316.50235	2124.29845	-5477.79995	6210.47315	-2619.42730
27	15	172.38841	-1365.63637	3797.82872	-4668.84297	2135.38996
27	16	-82.04318	521.72814	-1402.72026	1641.93116	-708.89756
27	17	213.68711	-1654.83759	4550.83331	-5527.65534	2499.19246
27	18	-61.53654	357.42980	-931.77652	1070.72926	-459.00037
27	19	22.82996	-233.68558	605.29669	-686.78711	287.79176
27	20	100.37878	-803.00138	2163.87346	-2569.98663	1135.12096
27	21	135.30542	-1013.75692	2623.67996	-2993.64232	1271.51933
27	22	-102.26459	672.33844	-1830.28773	2199.39695	-983.87353
27	23	23.53835	-225.26610	559.62153	-613.07136	250.36833
27	24	-1.11882	-57.90481	138.28271	-144.79466	56.46291
27	25	32.04628	-297.86360	790.85268	-930.92804	409.60176
27	26	69.31465	-553.41844	1451.95335	-1689.77419	734.47173
28	13	1299.25528	-9490.27278	25648.86571	-30648.20143	13641.98569
28	14	-802.71934	5557.13565	-14492.50127	16652.32101	-7131.75128
28	15	-687.13279	4815.36329	-12764.09874	14925.47544	-6502.97141
28	16	-83.87004	540.80866	-1473.85067	1751.56524	-769.49883
28	17	240.38913	-1862.45759	5147.55099	-6280.82270	2850.46336
28	18	98.28020	-783.32094	2100.90138	-2491.25483	1100.25249
28	19	-79.73095	477.21162	-1229.05508	1399.77358	-595.80520
28	20	-13.82647	6.37884	28.24605	-86.10292	60.58910
28	21	34.96131	-307.94475	779.25654	-872.88576	365.63719
28	22	-111.73851	706.83358	-1838.22256	2113.50246	-906.29693
28	23	-38.15494	203.70631	-558.13689	678.54704	-307.89243
28	24	41.96761	-358.86216	920.34225	-1042.63883	440.59229
28	25	-74.08759	452.96917	-1196.10645	1396.65687	-608.33477
28	26	-19.55386	84.83082	-265.86897	356.38318	-174.14555
28	27	14.10012	-161.67729	416.79129	-482.23615	209.63667
29	14	-3687.91939	26586.29961	-71551.51479	84931.03452	-37529.15361
29	15	-115.26009	669.41867	-1558.31499	1541.60820	-546.34580
29	16	-77.82295	531.92198	-1543.61938	1944.82964	-905.32983
29	17	98.79824	-788.15497	2123.84499	-2542.53468	1136.63155
29	18	-18.39892	73.16234	-231.48965	301.91536	-142.66903
29	19	-2.29085	-70.37705	213.68234	-279.62579	132.14602
29	20	50.83954	-445.86069	1207.46893	-1445.51969	644.42782
29	21	13.39323	-168.00370	435.22773	-492.51377	205.28332
29	22	13.25310	-154.34357	371.35056	-390.27849	151.00690
29	23	31.71807	-284.82206	713.35678	-783.76038	319.17186
29	24	-5.42174	-39.80088	115.54132	-143.13590	65.07054
29	25	89.92676	-723.30312	1942.33089	-2297.73341	1010.95066
29	26	-1.01853	-77.25547	239.32338	-320.80225	157.70297
29	27	29.24142	-261.91007	651.92207	-716.09648	292.63446
29	28	20.65785	-206.77619	531.59148	-610.45509	262.79670
30	15	686.85897	-5251.96300	14715.76888	-18182.68543	8339.44455
30	16	-739.12843	5448.07925	-15196.15711	18720.56007	-8601.32704
30	17	248.77297	-1843.54061	4887.76320	-5738.53239	2512.39513
30	18	-411.05425	2867.23696	-7633.90972	8948.68522	-3899.97404
30	19	-220.46556	1499.62736	-3980.47096	4647.22535	-2016.19387
30	20	-134.43569	849.34084	-2162.72014	2422.39527	-1008.77728
30	21	87.50545	-709.12233	1909.05043	-2269.26677	1004.59971
30	22	-170.90660	1147.35255	-3061.58708	3611.37845	-1588.84934
30	23	-28.85672	139.49839	-394.97811	494.67154	-230.78562
30	24	-60.37299	353.00562	-927.83172	1077.01521	-465.59503
30	25	91.13331	-735.07332	1982.71851	-2358.62793	1044.68384

30	26	6.92525	-117.36223	297.72476	-331.03366	136.54516
30	27	-94.28036	597.12720	-1580.83566	1852.05395	-810.00170
30	28	12.66036	-153.25507	387.11246	-431.26212	178.47883
30	29	92.84363	-720.43557	1894.41213	-2208.12355	960.96502
31	16	832.82257	-6197.54672	17007.03296	-20645.10307	9330.11469
31	17	-528.95235	3729.82714	-9985.49012	11776.25243	-5169.20395
31	18	-61.02001	364.77279	-986.16871	1172.07176	-521.33955
31	19	365.95090	-2758.68442	7528.20757	-9075.06266	4074.08709
31	20	430.06248	-3186.89912	8585.40718	-10213.74315	4525.16954
31	21	342.74403	-2504.36032	6610.21325	-7702.20804	3341.75424
31	22	-82.12378	511.45279	-1370.00053	1628.49452	-724.70165
31	23	104.44627	-823.77243	2192.49746	-2570.00324	1120.00820
31	24	-33.66681	166.46844	-449.53809	541.84306	-245.37822
31	25	86.04000	-693.96989	1861.96288	-2206.20376	974.35696
31	26	-73.45111	465.01240	-1275.22278	1543.64270	-695.08532
31	27	163.58913	-1228.99871	3240.77610	-3776.07958	1640.84078
31	28	-80.64374	511.42147	-1382.06941	1650.55333	-734.73488
31	29	1.13840	-85.26203	246.14737	-314.25132	148.95053
31	30	-30.81049	156.08225	-423.68369	503.09432	-222.30664
32	17	993.97902	-7253.02654	19503.65887	-23151.16468	10219.08316
32	18	118.92246	-995.96113	2865.69573	-3656.76977	1733.32300
32	19	233.92333	-1784.26845	4857.40483	-5854.00973	2630.15827
32	20	-249.30246	1707.32261	-4543.41381	5328.74685	-2328.55396
32	21	192.59056	-1463.95745	3930.73176	-4662.47322	2058.90970
32	22	-44.15924	210.44259	-480.64827	469.99401	-165.57663
32	23	-47.15283	285.82232	-826.65376	1049.66759	-494.68386
32	24	22.98953	-243.33063	652.35464	-766.45179	333.63398
32	25	2.93195	-99.25238	272.52622	-328.63037	147.24900
32	26	-38.92013	190.07446	-469.80364	511.10155	-206.12586
32	27	12.96148	-157.60480	394.25859	-431.04607	174.29531
32	28	29.82727	-288.84068	776.27829	-920.37021	406.67261
32	29	-20.41887	68.68939	-171.37268	191.46756	-81.02358
32	30	26.98017	-257.65888	671.75035	-775.20771	333.70799
32	31	23.56690	-210.69564	497.64234	-520.10637	202.12651
33	18	-884.17842	5904.52186	-14727.95064	16035.47328	-6433.32029
33	19	-40.03359	167.50315	-304.35156	152.53643	30.54057
33	20	227.63077	-1645.83233	4245.81869	-4856.10947	2073.39501
33	21	426.62150	-3215.77469	8811.65637	-10661.72318	4801.42793
33	22	107.30101	-831.86345	2193.60403	-2566.24910	1122.35330
33	23	-290.86459	1981.69491	-5225.17469	6088.39846	-2646.40017
33	24	39.62052	-332.14778	812.54387	-869.69485	342.86649
33	25	-41.22078	231.07339	-646.01644	795.70491	-364.21162
33	26	-47.50591	283.64198	-802.96787	997.58070	-458.85668
33	27	-227.13556	1524.64130	-3999.96870	4640.19262	-2007.83909
33	28	-86.07447	530.10205	-1380.25332	1586.93838	-679.54406
33	29	70.69789	-585.57220	1578.01691	-1875.39325	829.94184
33	30	-4.55074	-43.39452	126.56838	-160.71551	74.77369
33	31	61.63501	-505.06091	1330.31022	-1549.02830	672.11981
33	32	-80.03967	503.96600	-1339.55751	1567.23341	-682.75908
34	19	2003.88440	-14496.80557	38939.58738	-46268.79633	20497.67948
34	20	-640.69471	4274.64702	-10720.78134	11763.67452	-4770.35015
34	21	-205.18664	1483.68477	-4195.91658	5209.59345	-2401.62036
34	22	104.65830	-815.01243	2157.51660	-2538.96679	1117.22487
34	23	-200.54003	1402.40476	-3849.94219	4657.49239	-2098.00903
34	24	-154.52138	1047.08568	-2836.14612	3389.07910	-1508.51827
34	25	-132.05878	882.84535	-2389.69575	2855.62444	-1271.35083
34	26	-24.34434	82.70818	-175.38392	152.47212	-43.10709

34	27	-32.24849	158.87591	-430.13937	513.59212	-228.00740
34	28	48.50722	-403.96952	1032.20074	-1163.84441	489.37877
34	29	44.76333	-379.36348	969.40200	-1087.96072	453.15466
34	30	2.03608	-98.70163	293.18454	-379.10203	180.61906
34	31	31.46701	-290.85921	755.52378	-861.43046	363.53542
34	32	-64.29254	383.85814	-1006.58511	1162.44904	-499.38533
34	33	-5.45412	-18.47304	25.63894	-10.24239	-2.53790
35	20	253.93043	-2064.65196	6023.15003	-7779.14646	3733.89105
35	21	-57.71510	306.49005	-721.21753	709.10107	-242.83171
35	22	-390.47481	2707.03051	-7167.36509	8351.15082	-3617.88689
35	23	228.64797	-1722.82981	4630.43183	-5508.29554	2443.29822
35	24	17.01845	-243.82838	771.01003	-1048.94334	519.41209
35	25	-110.04165	671.43956	-1688.17188	1872.22039	-773.44875
35	26	9.64524	-162.07785	476.03918	-608.39890	285.70767
35	27	41.12512	-371.50103	989.15505	-1155.86316	500.79387
35	28	-76.37843	487.46056	-1342.01639	1630.47378	-737.00667
35	29	36.21525	-335.42705	896.36940	-1053.28702	459.76033
35	30	-86.97027	561.65674	-1533.24347	1849.04686	-830.50820
35	31	41.85396	-375.03753	1011.75026	-1209.13036	540.03795
35	32	39.59753	-347.58647	905.54642	-1039.87129	444.10646
35	33	88.25058	-697.05394	1846.90274	-2163.24329	944.37189
35	34	-2.39443	-54.31216	157.81770	-208.11269	102.35616
36	21	1791.95618	-13086.20114	35420.88008	-42357.48318	18860.18806
36	22	-387.34786	2754.35193	-7493.38606	8980.30489	-4006.23043
36	23	546.94766	-4010.48886	10763.98763	-12779.18981	5656.73984
36	24	-29.84909	144.93718	-403.87639	490.63204	-222.49827
36	25	170.05398	-1245.93187	3197.08185	-3619.37328	1523.50005
36	26	-34.55989	174.75069	-477.75765	579.41157	-263.78658
36	27	-107.05309	670.37920	-1732.89754	1976.00183	-839.37218
36	28	179.82345	-1339.14033	3510.43852	-4064.66003	1754.72858
36	29	-43.84877	214.34955	-504.63925	515.62914	-191.80447
36	30	-46.32410	274.92061	-778.22834	967.02983	-444.37813
36	31	-48.55308	267.00156	-694.73966	800.45924	-344.29437
36	32	-107.28854	697.10096	-1866.30708	2208.91606	-974.81187
36	33	-59.92559	341.42546	-871.93270	985.07046	-415.60245
36	34	-23.58603	103.09632	-288.14635	353.94567	-161.73742
36	35	52.20791	-432.02650	1132.28071	-1319.23996	574.68663
37	22	-201.06991	1235.63638	-2907.77072	2904.66731	-1031.60627
37	23	-81.13079	628.68140	-1993.99609	2694.59752	-1326.43015
37	24	52.04644	-429.01129	1092.95452	-1231.13929	512.84082
37	25	-46.24918	272.16336	-769.75688	952.40149	-438.29405
37	26	-118.97233	785.15463	-2118.38861	2519.99547	-1116.77095
37	27	68.63902	-561.54689	1489.45782	-1753.25954	772.04259
37	28	-48.20527	253.64889	-632.95152	693.10617	-281.08540
37	29	132.63558	-1015.37946	2688.00458	-3147.02202	1375.21651
37	30	-117.87971	759.13141	-2002.36731	2338.23079	-1019.69463
37	31	132.70309	-1022.32670	2719.75023	-3190.95355	1393.51490
37	32	-90.26916	559.08893	-1458.36398	1683.89667	-725.75575
37	33	0.40331	-80.06652	222.08605	-267.37459	118.53735
37	34	-24.34015	101.97259	-272.30861	323.00549	-143.63435
37	35	-73.94937	449.67594	-1176.44981	1359.56117	-586.24288
37	36	-19.35075	80.48522	-237.26905	298.31329	-137.57878
38	23	746.91650	-5546.84425	15125.86680	-18196.16289	8129.13591
38	24	393.67176	-3009.56106	8329.96057	-10167.56874	4612.53087
38	25	126.72996	-949.86743	2440.16282	-2765.46659	1163.41637
38	26	373.17431	-2775.45572	7480.06082	-8906.67009	3950.59483
38	27	-133.69754	855.14414	-2216.63516	2539.20240	-1086.15475

38	28	275.10093	-2065.10639	5553.57130	-6586.56133	2906.57139
38	29	30.77454	-304.43733	833.18085	-1004.77723	450.90540
38	30	-2.53594	-72.27399	232.87380	-320.43018	160.55944
38	31	102.90896	-806.46237	2135.00019	-2491.82577	1082.51845
38	32	-3.66852	-60.13679	189.89792	-253.65708	122.92593
38	33	76.50085	-616.53202	1634.06615	-1913.40908	835.46294
38	34	-50.84269	291.56491	-778.19700	917.36193	-402.83867
38	35	35.48367	-308.90395	778.30578	-862.46818	354.46947
38	36	-11.78698	14.89890	-42.12682	51.01662	-22.98932
38	37	-67.66903	427.42288	-1165.71127	1395.88760	-621.16214
39	24	-1004.20844	7182.64310	-19375.26819	23108.86487	-10293.65777
39	25	-523.85211	3694.28327	-9912.21765	11743.31793	-5189.96798
39	26	-24.10757	137.01103	-463.75773	645.71623	-323.62325
39	27	-227.34987	1561.50612	-4188.69820	4956.60041	-2185.98581
39	28	-21.48176	105.98404	-351.43591	487.19308	-244.43037
39	29	-113.36860	743.11730	-2001.12221	2378.89323	-1054.20939
39	30	-74.98983	461.21559	-1233.10548	1460.44437	-646.30888
39	31	-60.47147	356.63990	-947.74113	1112.70078	-486.79255
39	32	51.03164	-442.58811	1185.46498	-1398.83314	613.95958
39	33	91.87457	-739.68718	1993.10093	-2368.80866	1048.22574
39	34	-78.02798	495.49766	-1346.69406	1613.86738	-719.25624
39	35	31.34784	-286.19416	735.03053	-833.02679	351.99229
39	36	20.81054	-211.74872	541.95020	-612.24572	257.39269
39	37	-77.50114	496.44475	-1353.68006	1624.97828	-725.30571
39	38	-25.58817	123.14841	-345.33526	418.79495	-187.60554
40	25	1069.59793	-7894.95873	21476.62516	-25763.36016	11481.66608
40	26	-56.18405	341.12147	-969.74843	1230.36990	-592.15844
40	27	-149.30890	1017.13158	-2777.57061	3340.22900	-1495.31363
40	28	-56.33263	327.21543	-873.03354	1027.75776	-453.40080
40	29	68.14502	-587.66584	1634.03994	-2005.95670	915.34767
40	30	161.14610	-1227.48963	3271.31139	-3852.41011	1690.58021
40	31	-178.06053	1207.53677	-3241.31043	3839.76735	-1693.83674
40	32	242.62793	-1817.04547	4859.80050	-5738.82324	2524.59442
40	33	-71.44494	428.32465	-1121.51684	1298.44874	-560.30706
40	34	-10.38626	-6.22836	29.13216	-42.41183	19.90641
40	35	-10.00614	2.65384	-18.66689	35.82964	-21.32696
40	36	-79.79870	494.63765	-1307.00569	1524.05485	-661.69076
40	37	-14.34689	41.21162	-138.02204	196.32304	-101.29731
40	38	-5.91349	-23.82492	50.96239	-45.32257	12.96642
40	39	-12.02892	24.61317	-79.78424	103.84843	-48.73167
41	26	368.21074	-2832.37338	7888.10718	-9705.03168	4440.71222
41	27	-189.03555	1236.25334	-3189.63193	3628.80357	-1542.64144
41	28	154.25849	-1212.47265	3324.93660	-4031.07799	1818.33245
41	29	197.70627	-1526.15060	4174.79098	-5054.88893	2282.67613
41	30	-62.47110	367.43312	-972.55676	1139.68726	-500.24160
41	31	-10.09934	28.23911	-158.37253	281.58804	-164.21983
41	32	-75.70142	440.07071	-1105.47547	1225.30053	-506.07966
41	33	-122.96786	776.55711	-1995.34668	2262.95167	-956.00804
41	34	-148.34694	984.86238	-2623.16439	3089.05730	-1356.49059
41	35	-41.76206	246.50277	-717.12911	917.75589	-435.35744
41	36	-138.59803	924.47598	-2484.44368	2952.40869	-1308.40018
41	37	-16.77932	15.47323	41.40480	-142.22072	101.74300
41	38	29.46211	-270.92282	688.20915	-767.10465	316.39563
41	39	-54.44214	314.62457	-826.31280	956.47650	-412.44787
41	40	29.56067	-267.19888	685.74149	-786.31127	338.39307
42	27	44.94526	-362.55209	890.60161	-986.05843	409.62581
42	28	-563.30255	3925.16670	-10390.57532	12147.45631	-5297.42625

42	29	-305.80719	2115.22518	-5640.88996	6630.80172	-2901.68524
42	30	31.03836	-296.58032	790.53606	-936.73157	414.23755
42	31	-207.94477	1418.75898	-3807.49098	4518.46676	-2001.44210
42	32	-174.79044	1172.67815	-3125.45245	3684.13837	-1620.84427
42	33	100.55480	-758.78416	1926.49399	-2155.00411	896.30867
42	34	-100.96835	623.52512	-1602.89794	1822.96540	-774.01990
42	35	70.73480	-578.66925	1538.19165	-1806.03694	790.86799
42	36	120.71980	-937.66539	2500.67836	-2946.21420	1294.53171
42	37	17.07455	-182.96168	453.76689	-492.75555	197.71035
42	38	-16.08470	27.75649	-35.82318	-0.76853	18.38347
42	39	5.15276	-107.17696	281.54543	-326.20353	140.59465
42	40	-19.75986	67.29701	-168.77505	184.62143	-74.95105
42	41	-34.13099	179.75735	-488.66747	583.20098	-259.62147
43	28	-821.93244	6008.07920	-16615.57298	20326.65810	-9287.22942
43	29	402.29109	-2883.24058	7515.32052	-8672.90860	3734.52435
43	30	-196.69195	1316.76018	-3472.24641	4041.22366	-1755.40738
43	31	93.46073	-736.95511	1948.35304	-2281.53480	996.46839
43	32	245.91765	-1811.56804	4767.53177	-5541.39033	2398.81994
43	33	-126.99120	825.61448	-2182.25559	2548.05187	-1109.54156
43	34	149.16743	-1132.38142	2996.75922	-3507.90092	1532.48002
43	35	1.45895	-80.86955	201.05255	-215.90007	84.18378
43	36	-97.15019	607.98006	-1592.63618	1848.66838	-801.77570
43	37	13.64139	-177.65974	486.68006	-583.94410	259.73655
43	38	55.35123	-480.77319	1309.31426	-1570.63016	701.06734
43	39	-31.92125	137.28085	-321.35235	331.78512	-127.50381
43	40	-54.65299	314.15708	-824.04433	954.65079	-412.32020
43	41	-25.36375	118.87700	-337.46972	419.78638	-193.83682
43	42	19.18009	-193.57502	491.14882	-558.85827	239.06353
44	29	-387.32880	2797.56634	-7730.28216	9412.08900	-4268.53628
44	30	18.15433	-252.08032	809.26423	-1133.55696	579.57879
44	31	85.50051	-690.82821	1859.09386	-2221.75044	990.78720
44	32	-167.12979	1140.84526	-3088.29811	3676.82522	-1626.04667
44	33	231.61896	-1708.03551	4489.70744	-5213.74749	2255.73895
44	34	-38.52603	202.71988	-548.87355	656.77496	-293.13851
44	35	68.16926	-581.74668	1599.52505	-1939.26884	874.83246
44	36	47.86008	-407.48579	1058.14966	-1210.31760	514.77720
44	37	108.34978	-868.87804	2366.65127	-2843.95114	1272.60471
44	38	31.94741	-302.31518	803.84482	-942.08675	411.26949
44	39	2.39247	-96.18152	269.40328	-328.69958	147.98287
44	40	41.64192	-371.27329	987.86015	-1155.70826	501.80149
44	41	-17.24495	58.19916	-174.17345	229.30404	-112.12456
44	42	-90.80490	583.03671	-1563.89177	1850.79048	-816.18937
44	43	5.65452	-102.29685	262.30248	-306.78189	136.25620
45	30	301.10657	-2205.99534	5827.59449	-6818.65976	2974.82695
45	31	-353.99930	2488.13688	-6707.70093	7967.14866	-3522.08714
45	32	31.77274	-337.01278	986.83497	-1268.17068	601.38221
45	33	-82.11226	513.79697	-1392.69081	1684.71126	-767.79600
45	34	-51.36702	323.06607	-942.67381	1202.15654	-566.99511
45	35	-229.52646	1588.84248	-4291.59033	5115.18941	-2270.75632
45	36	-70.74887	415.74502	-1064.03583	1196.64145	-498.87605
45	37	2.71890	-100.59395	283.28631	-348.68957	158.86321
45	38	60.55372	-523.15917	1431.51538	-1722.77101	770.19576
45	39	66.55481	-531.05374	1368.00655	-1557.31700	661.53250
45	40	-115.73274	751.40680	-1995.65045	2343.04105	-1025.66761
45	41	85.02741	-690.62000	1867.60941	-2229.36712	991.01004
45	42	-110.65073	721.57770	-1929.79218	2282.12550	-1007.38706
45	43	41.22698	-350.77844	897.16284	-1013.87844	426.56360

45	44	-38.99421	220.48770	-609.63358	735.77720	-329.15335
46	31	-282.22651	1852.33732	-4700.05194	5250.57038	-2185.25727
46	32	37.55788	-336.51268	868.71994	-987.18367	412.42778
46	33	19.82159	-222.84341	605.59953	-730.03102	327.74504
46	34	-117.95697	753.34629	-1964.95795	2256.19787	-964.20014
46	35	292.43854	-2161.31045	5751.32879	-6770.10682	2973.81157
46	36	99.59761	-787.63803	2097.74324	-2466.92898	1080.44613
46	37	-164.90107	1122.01181	-3037.13862	3627.86271	-1613.22283
46	38	93.79646	-734.33591	1925.20322	-2226.85399	959.47603
46	39	-76.30036	442.42242	-1103.65459	1213.38680	-495.93207
46	40	-115.69721	754.24114	-2011.78273	2370.71949	-1041.08596
46	41	-7.69348	-32.30822	118.43244	-170.49694	85.72380
46	42	55.07026	-485.02298	1337.66561	-1621.61598	729.65309
46	43	-100.01374	622.00471	-1606.24833	1837.26869	-785.75568
46	44	-9.08648	-10.04382	37.87932	-57.02652	29.42459
46	45	39.86905	-340.76490	880.50015	-1013.12976	436.34996
47	32	231.98022	-1808.83178	5027.76154	-6177.92360	2824.43317
47	33	216.94938	-1630.04284	4351.23030	-5135.24921	2257.19695
47	34	120.82564	-927.10344	2438.49818	-2838.84219	1232.33566
47	35	153.12693	-1169.41295	3103.52479	-3629.99583	1578.34925
47	36	3.24160	-114.82293	350.63983	-467.42722	228.80915
47	37	-132.20828	865.31990	-2298.42441	2701.92113	-1186.56300
47	38	67.50743	-564.95150	1524.19034	-1817.17934	808.40097
47	39	8.50003	-152.07382	446.80812	-571.59526	269.55421
47	40	119.03031	-925.72983	2467.17962	-2902.88537	1272.77632
47	41	-115.74466	755.99179	-2024.12527	2398.24025	-1060.23435
47	42	-66.38583	393.93899	-1031.15026	1194.14282	-515.89203
47	43	-51.03563	302.57175	-832.31741	1009.73128	-455.75702
47	44	13.20258	-174.59822	486.06164	-593.84942	268.45976
47	45	-28.07756	125.22920	-319.37005	357.16701	-148.40176
47	46	-29.45485	146.41928	-396.12771	465.69606	-202.84093
48	33	0.19557	-86.86478	260.76519	-355.86752	179.11427
48	34	-51.72067	331.01303	-981.24911	1265.67065	-604.65515
48	35	-156.94654	1020.76799	-2652.65402	3039.64537	-1298.08365
48	36	142.20543	-1108.85419	2998.61446	-3584.34883	1596.72576
48	37	99.08152	-818.02187	2277.98286	-2805.96637	1288.18635
48	38	30.73965	-274.41847	679.98663	-746.01350	306.08715
48	39	-136.64170	895.28895	-2370.06989	2772.92819	-1209.35767
48	40	-12.37578	12.75964	-34.69204	45.20863	-22.71146
48	41	-52.59743	292.16711	-754.44242	862.20098	-367.80192
48	42	-26.56029	100.57891	-229.67441	230.06677	-85.05377
48	43	-51.14706	278.26034	-708.38816	800.75497	-338.81846
48	44	-32.37156	156.13772	-412.34533	485.82737	-215.12860
48	45	2.42978	-94.79959	266.25531	-326.91843	147.91513
48	46	-63.41395	376.90117	-987.16575	1139.75915	-490.23761
48	47	1.30369	-64.47508	143.32054	-145.00440	55.69646
49	34	389.48379	-2855.15095	7585.68149	-8901.44530	3888.80874
49	35	-162.89661	1067.21523	-2790.26855	3223.04767	-1392.23440
49	36	-16.21138	56.86524	-191.32737	263.71958	-131.04829
49	37	159.49523	-1230.01971	3315.46254	-3949.14076	1752.60118
49	38	-256.36422	1738.48527	-4589.17538	5357.48778	-2334.23804
49	39	247.42718	-1814.20791	4749.34066	-5485.80536	2359.16588
49	40	91.61256	-719.00727	1885.76073	-2183.37568	941.83834
49	41	13.73948	-163.52160	413.35598	-463.89215	195.59802
49	42	0.94077	-82.98117	223.08681	-260.79922	112.45251
49	43	-0.30436	-65.20503	154.20755	-154.55708	54.56160
49	44	17.51361	-207.64060	572.72671	-691.13640	308.84113

49	45	48.78916	-424.64611	1139.07631	-1347.42567	593.07954
49	46	-15.05631	36.79404	-99.59058	118.67869	-52.80854
49	47	45.77507	-387.79851	1009.37789	-1163.57617	500.48216
49	48	-103.24190	670.53158	-1784.74064	2091.70803	-912.60314
50	35	180.53465	-1349.92823	3545.78132	-4111.06303	1770.23879
50	36	73.67208	-560.12615	1383.53000	-1508.31452	609.14714
50	37	199.54424	-1484.24726	3905.09718	-4539.47774	1965.54946
50	38	204.16749	-1536.63768	4101.31658	-4840.60143	2130.25154
50	39	-28.88372	147.93919	-434.68697	553.14360	-259.02984
50	40	142.06899	-1086.12637	2884.66709	-3388.52135	1485.12859
50	41	101.03465	-772.65266	1995.38456	-2277.54166	969.85912
50	42	-283.85971	1953.15427	-5199.87480	6114.09358	-2678.33962
50	43	-16.04710	52.00583	-172.88277	248.33132	-129.88054
50	44	-163.68815	1071.41759	-2795.17352	3228.83062	-1393.17806
50	45	-108.58089	683.25794	-1770.19283	2028.15262	-867.02071
50	46	-63.85254	361.90729	-908.99427	1009.19074	-417.88116
50	47	66.83236	-549.86602	1466.16164	-1726.27223	756.98496
50	48	8.16595	-137.46266	389.45200	-486.47565	225.15381
50	49	29.85745	-258.53276	632.82171	-687.99594	279.08908